SYNTHESIS AND CHARACTERIZATION OF PORPHYRIN-BASED PHOTOSENSITIZERS FOR PHOTODYNAMIC THERAPY

A THESIS SUBMITTED TO
THE GRADUATE SCHOOL OF NATURAL AND APPLIED SCIENCES
OF
ANKARA UNIVERSITY

by

Can AKMAN

IN PARTIAL FULFILMENT OF THE REQUIREMENTS
FOR THE DEGREE OF
MASTER OF SCIENCE IN
BIOMEDICAL ENGINEERING

ANKARA
2026

ABSTRACT

Master's Thesis

SYNTHESIS AND CHARACTERIZATION OF PORPHYRIN-BASED PHOTOSENSITIZERS FOR PHOTODYNAMIC THERAPY

Can AKMAN

Ankara University
Graduate School of Natural and Applied Sciences
Department of Biomedical Engineering

Supervisor: Prof. Dr. Hilal GÖKTAŞ

Photodynamic Therapy (PDT) is a non-invasive method that provides better cosmetic outcomes than conventional treatments in skin cancers and can also be used in elderly patients; however, its effectiveness is limited due to the restricted tissue penetration of light, the absorption of melanin at wavelengths like those of the photosensitizer, and aggregation-induced changes in the optical properties of photosensitizers. In this thesis study, porphyrin-based copolymer thin films were synthesized using the Plasma-Enhanced Chemical Vapor Deposition (PECVD) method to overcome these limitations. Tetraphenylporphyrin (TPP) was copolymerized with the electron-donating monomers thiophene and pyrrole, and TPP-co-Thiophene/TPP-co-Pyrrole thin films were obtained in their pure forms without the use of any solvents.

As a result of the Ultraviolet-Visible spectroscopy analysis, it was determined that the TPP-co-Thiophene copolymer thin films exhibit absorption at a wavelength of 655 nm with an approximately 10 nm bathochromic shift in the Soret and Q bands. This critical finding indicates an increase in the conjugation length and demonstrates that light absorption in the visible region is enhanced in accordance with the objective of deep tissue penetration and will be less affected by the optical masking of melanin pigment. In TPP–co-Pyrrole films, the high reactivity and volatility the Pyrrole monomer resulted in a matrix-dominant structure that overshadowed the optical features of TPP. Considering the obtained data from other characterization methods, it has been demonstrated that the PECVD method is an effective technique for producing solvent-free photosensitizer films with homogeneous morphology and tunable optical properties suitable for PDT applications.

January 2026, 67 pages

Key Words: Photosensitizer, Plasma-Assisted Chemical Vapor Deposition, Skin Cancer, Porphyrin, Thin Film, Conjugated Polymers

ÖZET

Yüksek Lisans Tezi

FOTODİNAMİK TERAPİ İÇİN PORFİRİN BAZLI FOTOSENSİTİZERLERİN SENTEZ VE KARAKTERİZASYONLARI

Can AKMAN

Ankara Üniversitesi
Fen Bilimleri Enstitüsü
Biyomedikal Mühendisliği Anabilim Dalı

Danışman: Prof. Dr. Hilal GÖKTAŞ

Fotodinamik Terapi (FDT), cilt kanserlerinde geleneksel tedavilere kıyasla daha iyi kozmetik sonuçlar sunan ve yaşlı hastalarda da uygulanabilen non-invaziv bir yöntemdir; ancak etkinliği, ışığın dokuya sınırlı penetrasyonu, ışığın fotosensitizerlerin dalga boylarına benzer dalga boylarında melanin tarafından soğurulması ve fotosensitizerlerin optik özelliklerinde agregasyona bağlı değişimler nedeniyle kısıtlanmaktadır. Bu tez çalışmasında, bu sınırlamaların aşılması amacıyla porfirin bazlı kopolimer ince filmler Plazma Destekli Kimyasal Buhar Biriktirme (PDKBB) yöntemi kullanılarak sentezlenmiştir. Tetrafenilporfirin (TPP), elektron verici monomerler olan tiyofen ve pirol ile kopolimerize edilmiş ve herhangi bir çözücü kullanılmadan saf formda TPP-ko-Tiyofen / TPP-ko-Pirol ince filmleri elde edilmiştir.

Ultraviyole–Görünür bölge spektroskopisi analizi sonucunda, TPP–ko-Tiyofen kopolimer ince filmlerinin Soret ve Q bantlarında yaklaşık 10 nm'lik bir batokromik kayma ile 655 nm dalga boyunda soğurum gösterdiği belirlenmiştir. Bu kritik bulgu, konjugasyon uzunluğunun arttığını ve görünür bölgede ışık emiliminin, derin doku penetrasyonu hedefi doğrultusunda iyileştiğini ve melanin pigmentinin optik maskeleme etkisinden daha az etkileneceğini göstermektedir. TPP–ko-Pirol filmlerinde ise pirol monomerinin yüksek reaktivitesi ve uçuculuğu, TPP'nin optik özelliklerini baskılayan, matris dominant bir yapının oluşmasına neden olmuştur. Diğer karakterizasyon yöntemlerinden elde edilen veriler de dikkate alındığında, PDKBB yönteminin, FDT uygulamalarına uygun, homojen morfolojiye ve ayarlanabilir optik özelliklere sahip çözücü içermeyen fotosensitizer filmler üretmek için etkin bir teknik olduğu gösterilmiştir.

Ocak 2026, 67 sayfa

Anahtar Kelimeler: Fotosensitizer, Plazma Destekli Kimyasal Buhar Biriktirme, Cilt Kanseri, Porfirin, İnce Film, Konjuge Polimerler

FOREWORD AND ACKNOWLEDGEMENTS

I would like to express my sincere gratitude to my advisor, Prof. Dr. Hilal GÖKTAŞ, for his unwavering support and guidance throughout my research, and for the reassurance he provided whenever an issue that came up. I am deeply grateful that he accepted me into his group, despite my background in veterinary medicine, and gave me the opportunity to embark on this interdisciplinary journey. I hope that we will achieve many more successes and collaborate further research together in the future.

I would like to express my respect and gratitude to Prof. Dr. Hakan Kayı for his support in the DFT simulations of this study. I would also like to thank Res. Asst. Mustafa TÜFEKÇİ and Res. Asst. Sena HAMARAT for their invaluable support in the laboratory and for patiently answering every question I had as someone who joined the department later.

I offer my infinite thanks to my beloved family, my mother, Feriha AKMAN and my father, Şinasi AKMAN who have always been by my side during this process. Thank you for your unwavering support, for helping me stand up whenever I fell, for being a constant pillar of strength behind me, and for enabling me to pursue what makes me happy. I also send my love to my dear cat, Lina, who supported me by sitting on my lap throughout the writing of this thesis.

Finally, I would like to acknowledge the financial support provided by the TÜBİTAK Directorate of Science Fellowships and Grant Programmes under the 2211-National Graduate Scholarship Program during the preparation of this thesis.

Can AKMAN
Ankara, January 2026

TABLE OF CONTENTS

SYMBOLS AND ABBREVIATIONS

°C	Degree Celsius
A.U.	Arbitrary Unit
ACQ	Aggregation-Caused Quenching
AFM	Atomic Force Microscopy
AK	Actinic Keratosis
ALA	aminolevulinic acid
BCC	Basal Cell Carcinoma
BD	Bowen's disease
Cm	Centimeter
CVD	Chemical Vapor Deposition
FTIR	Fourier Transform Infrared Spectroscopy
g	Gram
kJ	Kilojoule
MAL	Methyl Aminolevulinate
mTorr	Millitorr
NIR	Near-Infrared
Nm	Nanometer
NMSC	Non-melanoma Skin Cancers
PDT	Photodynamic Therapy
PECVD	Plasma Enhenced Chemical Vapor Deposition
PpIX	protoporphyrin IX
PPy	Polypyrrole
PS	Photosensitizer
PTH	Polythiophene
ROS	Reactive Oxygen Species
SCC	Squamous Cell Carcinoma
SEM	Scanning Electron Microscopy
TPP	Tetraphenylporphyrin
UV-Vis	Ultraviolet-Visible Spectrophotometry
W	Watt
XPS	X-Ray Photon Spectroscopy

LIST OF FIGURES

LIST OF TABLES

1. INTRODUCTION

The incidence of skin cancers is increasing in our country and around the world. Current treatment methods have side effects that are difficult to avoid and cosmetic consequences that cause concern in people's daily lives. Currently, the treatment methods used in the literature include surgical intervention, radiotherapy, chemotherapy, photodynamic therapy (PDT), immunotherapy, and chemical skin cleansing (National Cancer Institute, 2021). With economic and sociocultural developments, patients are looking for treatments with minimal side effects and satisfactory cosmetic results. Especially in elderly patients where surgical intervention is very limited or in cases where the patient is hesitant, the availability of alternative treatment methods is an important factor in the treatment and recovery processes of patients. The harmful effects of these other methods not only on cancerous tissues but also on healthy tissues limit patients' choice of the right treatment in today's conditions.

PDT has been approved worldwide as a treatment modality for pre-malignant and malignant non-melanoma skin cancers due to its non-invasive procedure, increased tumor selectivity, good cosmetic results and broad treatment spectrum. PDT offers treatment based on the principle of light and its absorption under tissue. The treatment uses photosensitizing agents that react (absorb) to light of a specific wavelength sent from outside when delivered under tissue. These agents are sensitive to different wavelengths depending on the location of the cancerous structures under the tissue. The light source used can also reach different distances under the tissue depending on the wavelength, for example, wavelengths of 630-700 nm in red light therapy, 540-570 nm in green light and 400-450 nm in blue light therapy (Broekgaarden et al., 2022; Dougherty et al., 1998).

However, the inadequate sub-tissue penetration of photosensitizers (PS) after topical application of PDT to the treatment area and the wavelength at which they are stimulated is around 600 nm limit the widespread use and efficacy of the treatment. PSs have limited skin penetration due to their physicochemical properties and can currently only be used in superficial lesions. The fact that the absorption wavelength of clinically approved PSs is around 600 nm affects the tissue penetration of light, and this again causes the treatment

to remain superficial. At the same time, the fact that the PS used, and melanin pigment absorb in a similar spectrum significantly reduces the effectiveness of the treatment in melanoma cancer, pigmented basal cell carcinoma and people with dark skin tone. The reason for this is that melanin can act as an optical shield preventing light penetration into the lesion, as melanin is known to be a dominant absorber at wavelengths between 500–600 nm (Sharma et al., 2015). In this case, it can be stated that in melanoma, light transmittance in the presence of melanin occurs only at wavelengths above approximately 650 nm. Many commercially available photosensitizers, such as Photofrin and Chlorin e6, belong to the porphyrin-based family, which will also be used in this thesis, and demonstrate their effectiveness when stimulated at the 630 nm level. In the context of melanoma treatment, the effectiveness of PSs is significantly hindered due to melanin-induced interaction (Juvekar et al., 2024).

By copolymerizing the two basic materials to solve the mentioned problem, the high wavelength absorption of PSs enabled the treatment of deeper, cancerous tissues without damaging healthy tissues. In a study conducted in 2022, it was shown that thin films of tetraphenylporphyrin (TPP) molecule produced by spin coating method were unstable when exposed to water, but thin films produced by physical vapor deposition method were stable in aqueous media (Gibbons et al., 2022). In this thesis, TPP copolymer was purely coated without solvent using plasma-containing methods based on the Chemical Vapor Deposition (CVD) system and its efficiency was measured. The coatings produced by PECVD consist of nanometer thin films of copolymerized TPP-co-pyrrole and TPP-co-thiophene molecule. Thanks to the ionized excitation and polymerization mechanism provided by the plasma, it formed cross-links on the coated surface. Since this cross-linked structure has high stability and integrity compared to other known bond types, it was prevented from separating or dissolving on the surface it bonds (Ravve, 2013; Shabbir et al., 2019). Copolymer thin film synthesis was performed by Plasma Enhanced Chemical Vapor Deposition (PECVD) method. Synthesis details and properties were detailed in this and the following sections. The vapor deposition method is a method used to deposit the targeted monomer material as thin films on the desired surface without using any 'solvent' in the film synthesis and polymerization process in the system (Dianatdar et al., 2023). With the plasma power used at different levels in the PECVD

method, the monomer molecules delivered to the system were excited to high energy levels. As a result of this excitation, the monomer molecules, which become unstable, radicalic and fragmented, formed polymerized structures by bonding with each other at different chain lengths to return to the stable structure (N. K. Jain et al., 2017).

The main objective of this thesis is to produce materials that absorb at longer wavelengths than conventional photosensitizers for use in photodynamic therapy in pigmented cancers. Two main limitations were addressed by attempting to red shift the absorption wavelengths of photosensitizers: (1) the penetration of light into the skin, and (2) the competition between the absorption spectrum of melanin pigment and that of conventional photosensitizers. At the same time, the photosensitizers were synthesized in a polymerized thin-film form to mitigate the aggregation-caused quenching (ACQ) effect. In this context, PECVD, a solvent-free and "green" fabrication method, was employed to enable the synthesis of pure materials. Tetraphenylporphyrin (TPP), a porphyrin derivative currently used in photodynamic therapy, and the electron-donating monomers pyrrole and thiophene were used to polymerize TPP. As a result, TPP-co-thiophene and TPP-co-pyrrole thin films were successfully fabricated and characterized. To evaluate the optical performance of the synthesized photosensitizers, UV–Vis analyses were conducted, and a 10 nm red shift was achieved in the TPP-co-thiophene films, resulting in absorption at 655 nm.

2. LITERATURE REVIEW

2.1 Skin Cancers

Skin cancer is a serious health problem that is prevalent, has an increasing incidence, and imposes a substantial financial burden on society (Sümen et al., 2018). Non-melanoma skin cancers (NMSC), such as squamous cell carcinoma (SCC) and basal cell carcinoma (BCC), are the most common malignancies in the United States (Figure 2.1). Approximately 3.5 million new cases are diagnosed annually, and the incidence is steadily increasing. Basal cell carcinoma constitutes the vast majority of NMSC, accounting for 75% of all NMSC cases, while SCC accounts for 20% (Neville et al., 2007). Although melanoma is relatively rare, it is the deadliest form of skin cancer. In the United States, approximately 60,000 people are diagnosed annually, while 8,600 people lose their lives to this disease. Skin cancers impose a financial burden during the treatment phase and lead to a loss of workforce (Kasap et al., 2015). A study conducted by Zoe Kao and colleagues in the USA in 2022 revealed that the prevalence and cost of skin cancer treatment are at significant levels; it affects 6.1 million U.S. adults with a total annual cost of $8.9 billion, and these figures are increasingly rising (Kao et al., 2023). Figure 2.1 shows the cancer incidence rates in the USA. Of the 6 million new cancer cases in the USA, 5.4 million are non-melanoma skin cancers (Gareau et al., 2017).

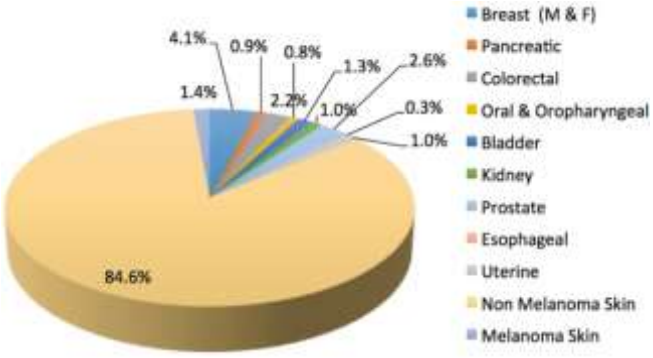

Figure 2.1 Cancers and rates in the USA (Gareau et al., 2017)

Eighty percent of skin cancers are diagnosed in patients aged 55 and older. A significant increase in the incidence of skin cancers has been observed in conjunction with the progressive aging of the European population. This increase is evident across all age

groups, regardless of gender (Ciążyńska et al., 2021). Non-melanoma skin cancers are the most common cancers among the caucasian population, and their incidence is rising globally. Melanoma, one of the most dangerous and lethal forms of skin cancer, is considered resistant to both radiotherapy and chemotherapy. Melanoma has become a significant public health issue due to its continuously increasing incidence over the last few decades and a 5-year survival rate that remains below 5%. While detection of the disease at an early stage can increase the chances of successful treatment, late-stage metastatic disease that has spread to other organs carries a poor prognosis, with a median survival time of less than 10 months. Melanoma is the cancer type with the most rapidly increasing incidence among all cancers (Kalal et al., 2017). Globally, 65,000 people die from skin cancers annually (Simões et al., 2015).

2.1.1 Melanoma in Türkiye

Melanoma occurs with the malignant transformation of melanocytes and is considered a neural crest neoplasia. It is rare compared to BCC and SCC but is very important due to its high mortality. It is the most aggressive and has the highest mortality among all skin cancers. Embryologically, melanocytes originate from the neural crest and colonize the skin, eyes, and various tissues during development. Benign proliferation of melanocytes is frequently seen and results in melanocytic nevi. However, with the presence of various mutations, aberrations, translocations, and deletions, malignant transformation to various melanoma types can occur.

Data regarding the epidemiological data and clinical features of melanoma in our country are limited. According to Turkey Cancer Registry Centers data, the number of cases diagnosed with cutaneous melanoma was reported to be 330 in 2011, 620 in 2012, 681 in 2013, 610 in 2014, and 618 in 2015, totaling 2859 between the years 2011-2015. The 2015 cutaneous melanoma incidence in our country was determined to be 1.5/100,000 person-years in men and 1.4/100,000 person-years in women (Acer and Kaya Erdoğan, 2019). In a single-center study conducted in our country where 19-year records were evaluated, frequently seen melanoma types were listed as superficial spreading melanoma (37.9%), lentigo maligna melanoma (31.64%), acral lentiginous melanoma (19.32%), and

nodular melanoma (6.76%). It was reported that the most frequently involved area was the head and neck region (34.78%) (Abali et al., 2015). In multi-center studies reported from our country, however, it was determined that the most frequently involved areas were the lower extremities and head-neck region respectively, and the most common subtypes were superficial spreading melanoma and nodular melanoma respectively. Furthermore, the male/female ratio was reported as 1.15, and the average age of diagnosis as 56.7. In the same study, only 8% of melanoma cases were determined to be in situ melanoma, and 92% as invasive melanoma (Gamsizkan et al., 2014).

2.1.2 Treatment methods for pigmented skin cancers and their limitations

Along with economic and social developments, the search for good cosmetic outcomes in treatments is increasingly rising. Research and development activities continue for tumor treatments that have lower recurrence rates, less pain, fewer side effects, and do not cause resistance after multiple treatments (Lu et al., 2014). Current skin cancer management strategies encompass a range of options including surgical interventions, radiotherapy, systemic chemotherapy, and topical pharmacological treatments. Treatment choice is influenced by various factors such as the location, size, and histological subtype of the tumor, the patient's general health, and the dermatologist's experience (S. Kim et al., 2023). The advantages and disadvantages of the treatments are given in Table 2.1. Radiotherapy and systemic chemotherapy are generally preferred in advanced cases or situations where surgery is not suitable (Souto et al., 2022). Although the surgical method is the gold standard for NMSC treatment, many patients are concerned about aesthetic effects in visible areas such as the face (E. H. Lee et al., 2016). Furthermore, radiotherapy has disadvantages such as high treatment frequency and long treatment duration, and has side effects such as dermatitis, hair loss, and skin thinning (Khong et al., 2020).

Chemotherapy, on the other hand, is a systemic treatment that affects the whole body. It can also affect healthy cells and cause various side effects. Common side effects include increased sensitivity to sunlight, skin discoloration or scarring, increased risk of infection (due to a decrease in antibody count), easy bruising or bleeding (due to a decrease in platelet count), fatigue or dizziness (due to a decrease in red blood cell count), alopecia

(hair loss), loss of appetite, dryness at nail edges, diarrhea and constipation, nausea, and vomiting (Satyanarayana Reddy Karri et al., 2017). Mohs micrographic surgery is a special excision method that provides the lowest recurrence rate for both primary and recurrent tumors in the treatment of high-risk non-melanoma skin cancers, but it is not routinely applied in Turkey (Elçin, 2015a). The disadvantages of the method are that it is a time-consuming and labor-intensive procedure. The success of the method is closely related to the experience of the doctors performing the excisional biopsy and evaluating the pathology, as well as the experience of the histotechnician preparing the horizontal frozen sections (Elçin, 2015b).

Additionally, methods such as curettage and electrodesiccation and cryotherapy are not suitable for the treatment of tumors in cosmetically sensitive areas and may cause permanent disfigurement (Kauvar et al., 2015). In a study conducted by Sotiriou et al. in 2015 with 44 patients with BCC, SCC, and actinic keratosis, imiquimod 5% cream was compared with Photodynamic Therapy. While no significant difference was found in treatment efficacy between them, the treatment preference of 59.09% of the patients was in favor of PDT. Furthermore, it was observed that patients preferred PDT as their choice for future treatment (Sotiriou et al., 2015).

Table 2.1 Comparison of treatment methods (Fırnhaber, 2012; Kauvar et al., 2015; Kong and Chen, 2022)

Treatment	Advantages	Disadvantages
Curettage and Electrodesiccation, Cryotherapy	Minimal equipment requirement, normal tissues are preserved.	Lack of histological margin control; slow healing; suboptimal scarring; intensive wound care required.
Excision	Histological margin control; rapid healing.	Deficiency in the preservation of healthy tissue (requires removing a margin of healthy skin).
Mohs Surgery	Microscopic margin control; preservation of healthy tissue; high cure rate.	High cost; low accessibility/availability.
Radiotherapy	Applicable when surgery is not possible.	High cost; frequency of treatment sessions; unsuitable for young patients; higher probability of recurrence compared to other methods.
Photodynamic Therapy	Local treatment; good cosmetic results; minimal damage to healthy tissue; no development of resistance in the tumor.	Low depth of tissue and light penetration.

2.2 Photodynamic Therapy as a Therapeutic Modality

Considering all these limitations, photodynamic therapy has been approved worldwide for treating superficial non-melanoma skin cancers due to its non-invasive procedure, increased tumor selectivity, good cosmetic outcomes, and broad treatment spectrum (Morton et al., 2019; Vianna Lopez et al., 2004). However, the use of PDT in melanoma treatment is limited for various reasons, and this study aims to provide a solution to these limitations.

In a 10-year study conducted between 2003 and 2013, more than 550 patients with a mean age of 72 were treated with Methyl aminolevulinate (MAL)-PDT. The patient population consisted of 67% with actinic keratosis (AK), 27% with BCC, and 4% with Bowen's disease (BD). As a result of a mean follow-up of 5.5 years, 99.5% of the lesions were cleared. The study demonstrated the superiority and low recurrence rate of MAL-PDT in treating AK, BCC, and BD (Brito et al., 2016).

Many studies have shown that PDT, not only alone but also in combination therapies with methods such as imiquimod, standard surgical excision, CO_2 laser, and radiotherapy, increases efficacy, improves cosmetic outcomes, and reduces side effects by lowering the radiation dose used in methods like radiotherapy (Cai et al., 2015; Lu et al., 2014; Nakano et al., 2011; Sotiriou et al., 2011; Zhang et al., 2018). Furthermore, in a study investigating the neoadjuvant use of PDT in 33 BCC and 26 SCC patients, it was observed that 22 patients recovered without the need for surgical intervention, and a mean reduction of 88% was seen in the lesions of the remaining patients. With this study, it was demonstrated that neoadjuvant PDT can significantly reduce tumor burden and allow for less morbid surgical excisions with histologically clear margins (Jeremic et al., 2011).

2.2.1 Photochemical mechanisms of PDT

In photodynamic therapy, photosensitizers, visible light, and oxygen are three fundamental components, and the combined use of these three causes tumor necrosis (tissue death) and apoptosis (programmed cell death). The working principle is simply

shown in Figure 2.2. The PS is excited at specific wavelengths containing the absorption peaks of a PS in visible light, usually containing red or blue light, near-infrared light (NIR), and even sunlight. Several photo-processes occur immediately after photon absorption, but the most probable deactivation pathway is the relaxation of the initial excited state to the lowest vibrational energy level.

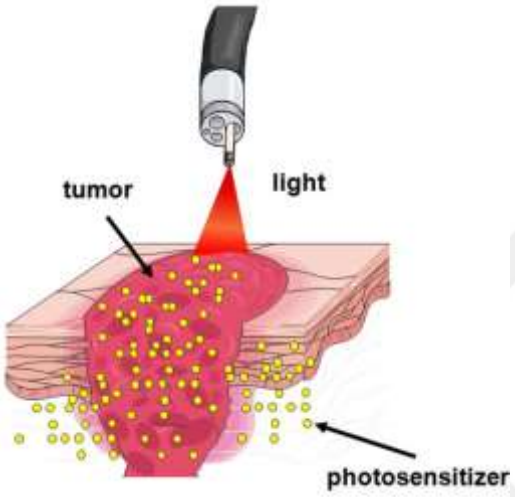

Figure 2.2 Overview of PDT. Following photosensitizer administration it undergoes systemic distribution and selectively accumulates in the tumor. Illumination activates the photosensitizer and in the presence of molecular oxygen triggers a photochemical reaction that culminates in the production of $^1O_2$ (Wachowska et al., 2011)

This very fast process (10^{-15} s) is defined as either internal conversion or vibrational relaxation. An excited molecule resides in the lowest excited singlet state on the order of nanoseconds before returning to the ground state. If the relaxation from this excited singlet state is accompanied by a photon emission, fluorescence occurs. Another relaxation pathway involves the occurrence of a non-radiative process known as intersystem crossing toward the lowest excited triplet state.

The photosensitizer in the excited triplet state (PS*) undergoes two types of reactions. In the Type I reaction, the excited PS reacts with biomolecules to produce superoxide anion radical ($O_2\cdot-$) and hydroperoxyl radical ($HO_2\cdot$) via electron transfer. $O_2\cdot-$ undergoes disproportionation to form hydrogen peroxide (H_2O_2), which is the precursor of the highly reactive hydroxyl radical ($OH\cdot$). $OH\cdot$ is chemically extremely reactive to almost all

biological molecules. In the Type II reaction, the excited PS produces singlet oxygen ($^1O_2$) through direct energy transfer to molecular oxygen. Singlet oxygen is highly reactive, like the hydroxyl radical, as illustrated in Figure 2.3. Both reactions can occur simultaneously, and the reaction rate depends on the type of PS used and oxygen concentrations. However, the Type II reaction is the primary mechanism of O_2-dependent PDT (Castano et al., 2004; Ding et al., 2011; Zhuang et al., 2020).

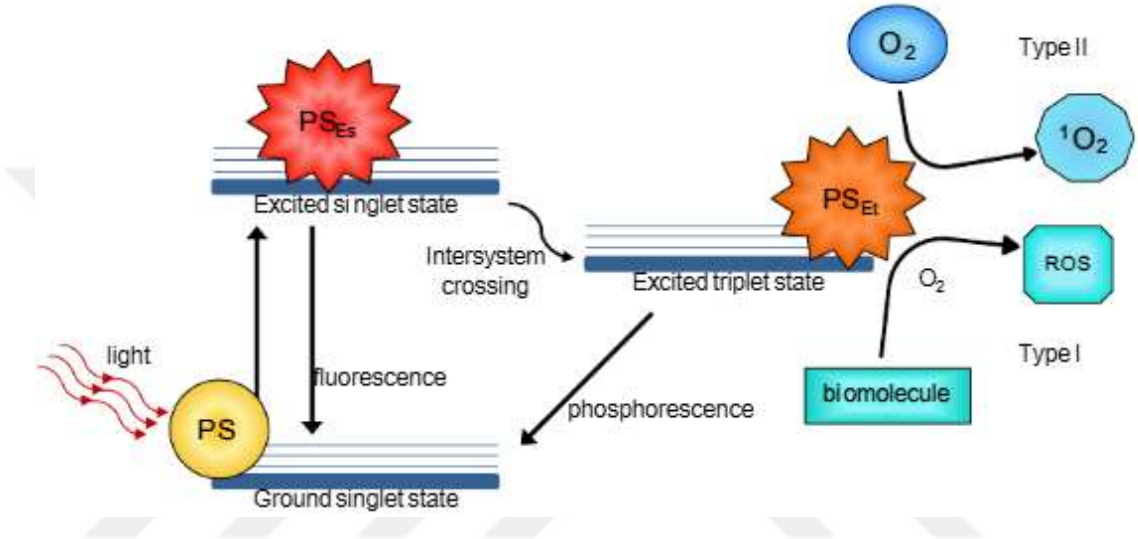

Figure 2.3 Type I and type II reactions in PDT (Calixto et al., 2016)

The generated reactive oxygen species (ROS) cause cell death via apoptosis or necrosis. The antitumor effects of PDT consist of three main mechanisms: direct cytotoxic effect on tumor cells, damage to the tumor vasculature, and stimulation of systemic immunity. The contribution of these mechanisms depends on the type and dose of PS used, the time between PS application and light exposure, light intensity and wavelength, and oxygen concentration. Therefore, a coordinated interdisciplinary effort is required to determine optimal PDT conditions (Agostinis et al., 2011).

2.3 Traditional Photosensitizers and Limitations

Hematoporphyrin and its derivatives are the first generation of PS. Hematoporphyrin was isolated by Schere in 1841 from the hemoglobin of red blood cells via treatment with concentrated sulfuric acid. Later, hematoporphyrin was further purified in the form of

photofrin. The first generation of PS was widely used clinically in the treatment of different cancers. However, there were some limitations and disadvantages such as low chemical purity, short wavelength of absorbed light, long half-life, and high accumulation in normal tissues, which led to a toxic effect on tissues directly related to the level of photosensitivity (Gelfuso et al., 2011).

Second-generation PSs were developed in terms of purity, long-wavelength absorption, photosensitivity, and tissue selectivity. Second-generation PSs overcame several serious disadvantages that arose from the use of first-generation PSs. First-generation PSs are not very specific to cancer cells and tend to accumulate in normal tissues as well. First-generation PSs are not cleared rapidly from the human body and lack sensitivity. Second-generation PSs are more effective and technically superior to first-generation PSs. Most second-generation PSs are based on porphyrin and chlorin structures. Second-generation PSs are excited at a long wavelength; therefore, they offer treatment opportunities with higher efficacy along with deeper light penetration. Third-generation PSs are being developed but are currently not efficient. They focus on tumor selectivity and photo-activation at long wavelengths. Topical application of PSs is suitable for the treatment of skin tumors with PDT as it delivers the drug to the pathological site, increasing the local bioavailability of the PS and reducing the occurrence of systemic side effects during treatment (Pucelik et al., 2016; Rocha et al., 2015; Gelfuso et al., 2011).

2.3.1 Wavelength dependence and tissue penetration in PDT

However, one of the major limitations in skin cancer treatment with photodynamic therapy is the penetration depth of light. Figure 2.4 shows the relationship between light wavelengths and skin penetration. In conventional Photodynamic Therapy, a prodrug, aminolevulinic acid (ALA), or its methyl ester, methyl aminolevulinate, is used, but they have some disadvantages. Since ALA is a prodrug, it has a long incubation period. After an incubation period of approximately 3 hours, the metabolic product protoporphyrin IX (PpIX) accumulates in the cell mitochondria. PpIX is activated by light at specific wavelengths (PpIX has absorption peaks at 405, 510, 545, 580, and 635 nm). The Soret band of PpIX is 405 nm, but a light source of 635 nm is generally used in clinics for the

purpose of deep light penetration. Following light exposure, reactive oxygen species (ROS) via the Type I reaction and singlet oxygen via the Type II reaction cause cell death. The depth is 1-2 mm with blue light and 1-6 mm with red light, which limits the use of PDT to more superficial skin lesions (C. N. Lee et al., 2020).

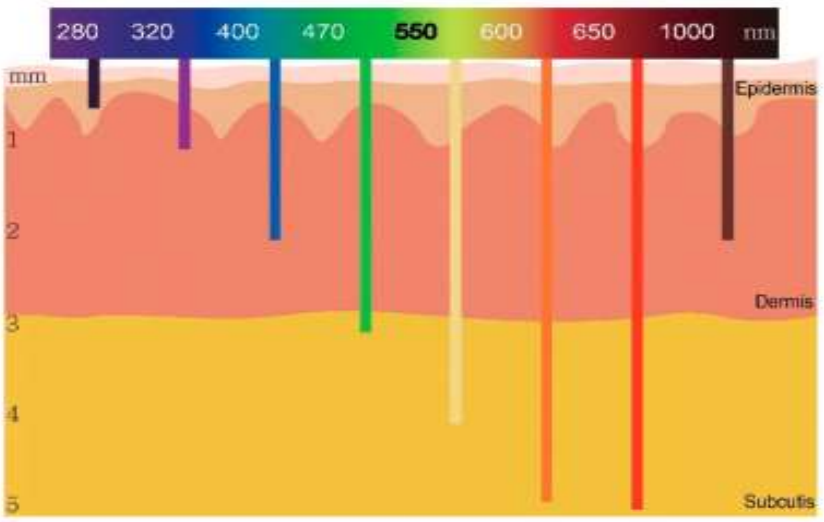

Figure 2.4 The relationship between the wavelength of light and skin penetration depth (C. N. Lee et al., 2020)

Additionally, in topical ALA-PDT applications, the tissue distribution of porphyrins induced by ALA is not homogeneous (Fritsch et al., 1998). There are many variables regarding the local bioavailability of PpIX. These include irregular ALA skin penetration, dependence on the amount of prodrug able to cross the skin, and the heterogeneous distribution of ALA-induced PpIX in the tumor. Therefore, the direct application of a PS instead of a prodrug may be advantageous, as the drug will already be photosensitive and will not be dependent on skin metabolism for conversion into an active molecule (Gelfuso et al., 2011).

Another disadvantage of the absorption peaks of conventional PDT agents being around 600 nm causes melanoma treatment to be resistant to PDT. The absorption spectrum of melanin is shown in Figure 2.5. The melanin pigment has been reported to be responsible for resistance to PDT in melanoma. The reason for this is that melanin can act as an optical shield preventing light penetration into the lesion, as melanin is known to be a dominant absorber at wavelengths between 500–600 nm (Sharma et al., 2015). In this

case, it can be stated that in melanoma, light transmittance in the presence of melanin occurs only at wavelengths above approximately 650 nm. Additionally, pigmented BCC responds more inefficiently to treatment due to light absorption by melanin (Lucena et al., 2015). For this reason, within the scope of this study, we aimed to shift the absorption peaks of 5,10,15,20-(Tetraphenyl)porphyrin to near infrared regions.

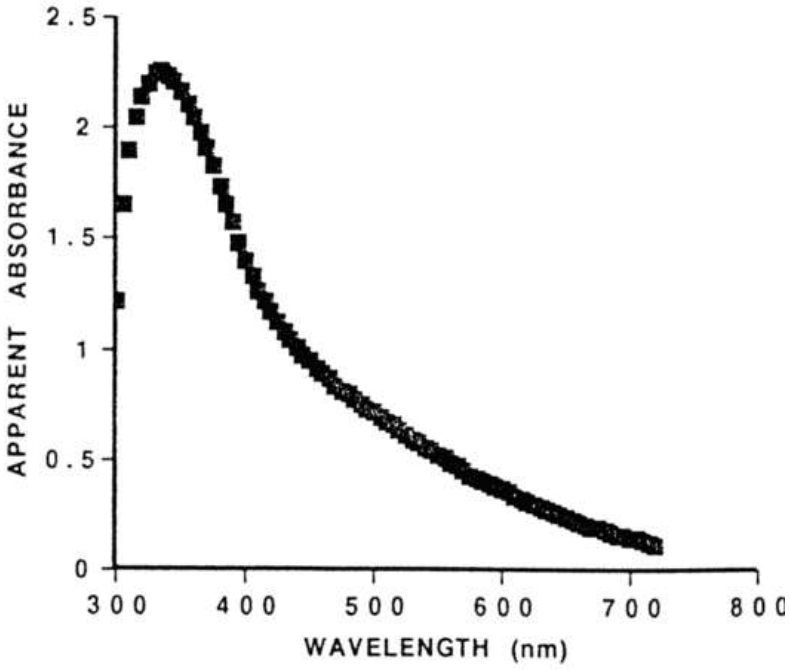

Figure 2.5 Absorption spectrum of melanin (Ross et al., 2009)

2.4 Conjugated Polymers for PDT

Various molecules such as porphyrins, chlorins, methylene blue, and phthalocyanines have been developed for PDT, and some porphyrin and chlorin derivatives have been systematically used in clinical applications. However, their mediocre light-harvesting capacities lead to limited singlet oxygen generation in tumor regions, and this situation hinders their use in clinical treatments. Therefore, increasing the photosensitization efficiencies of PSs is quite important for improving PDT efficacy. Conjugated polymers are a class of macromolecules possessing π–π conjugated systems in their chains, which enhances their light-harvesting capabilities compared to small molecule structures. This molecular wire effect is a characteristic of conjugated polymers, where excitons can

migrate effectively along the conjugated chain when excited, increasing the energy transfer efficiency to low-energy acceptors. The photosensitization efficiencies of PSs with a conjugated backbone can be significantly improved due to their excellent light-harvesting abilities and efficient energy transfer, which increases PDT efficacy (Lu et al., 2022).

Additionally, since porphyrins are typically planar and aromatic molecules possessing hydrophobic properties, the π–π stacking between them is very strong. This will lead to the aggregation-caused quenching (ACQ) effect (Yuan et al., 2010; K. Zhang et al., 2019). The ACQ effect inevitably reduces singlet oxygen generation and weakens PDT efficacy. In a study conducted by Zheng et al., it was observed that polymeric porphyrins reduced the ACQ effect and thereby increased in vivo PDT efficacy (Zheng et al., 2021). The optical absorption of porphyrins can be shifted to the near infrared (NIR) region by conjugating the porphyrin core to more aromatic systems (Bengasi et al., 2019). In this study, tetraphenylporphyrin, thiophene, and pyrrole have been used successfully for this purpose. The general properties of these molecules are given below.

The basic structure of porphyrin consists of four pyrrole subunits linked by methine bridges. The porphyrin skeleton possesses an extended π-conjugation system with 18 π-electrons, providing a wide wavelength range for light absorption (Makhlouf et al., 2014). Tetraphenylporphyrin (TPP) is a metal-free porphyrin derivative and is centrosymmetric with 4 phenyl groups, as shown in Figure 2.6. Tetraphenylporphyrin is a widely used benchmark molecule in various photochemical studies due to its facile synthetic access, rich visible-region spectrum, and broad structural analogy to chlorophylls. However, literature values for each key photophysical parameter vary over a wide range (Taniguchi et al., 2021).

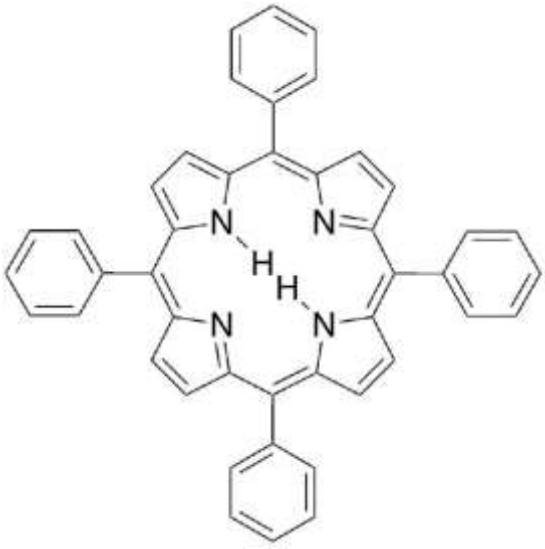

Figure 2.6 Chemical structure of TPP

Thiophene is a structure belonging to the class of heterocyclic compounds consisting of a five-membered ring containing one sulfur as a heteroatom, with the formula C_4H_4S. In medicinal chemistry, thiophene and its derivatives are used in therapeutic applications and studies. Due to its pi electron cloud, it behaves like an extremely reactive benzene derivative. The sulfur atom in this five-membered ring acts as an electron-donating heteroatom by contributing two electrons to the aromatic ring; therefore, it is considered an electron-rich heterocyclic compound (Bak et al., 1961; Mishra et al., 2011). Furthermore, it has been demonstrated through chemically synthesized porphyrin-thiophene oligomers that the absorption spectrum can be red-shifted in structures formed by linking porphyrins with thiophene bridges (Odobel et al., 2002). Its chemical structure is shown in Figure 2.7.

Figure 2.7 Chemical structure of thiophene

Pyrrole is a 5-membered aromatic nitrogen-containing heterocycle, like thiophene, that is ubiquitous in compounds of biological and material significance. It is the key structural

component of compounds crucial for life, such as chlorophylls and hemes, and is also an important building block for conjugated polymer studies. Pyrrole is widely known as a biologically active scaffold possessing a diverse range of activities. Pyrrole-containing analogs are considered a potential source of biologically active compounds that harbor a significant set of advantageous properties and can be found in many natural products (Bhardwaj et al., 2015; Philkhana et al., 2021). Chemical structure of Pyrrole shown in Figure 2.8.

Figure 2.8 Chemical structure of pyrrole

Considering the disadvantages of ALA-PDT, it was predicted that the use of a direct PS instead of a PS precursor and the proximity of the absorption spectrum of the used PS to the NIR region would improve the treatment. Therefore, within the scope of this study, the synthesis of thin films (80 ± 20 nm) was performed by copolymerizing the electro-donor 5,10,15,20-(Tetraphenyl)porphyrin [TPP] monomer with thiophene and pyrrole, which act as electron acceptors relative to TPP in this system, and the efficacy of these PSs for PDT was investigated by measuring UV-Vis analysis.

2.5 Plasma Enhanced Chemical Vapor Deposition

Since such structures cannot be synthesized in a pure state and homogeneously on every surface using conventional wet methods such as chemical and electrochemical techniques, within the scope of this study, PSs were synthesized under vacuum using the Plasma Enhanced Chemical Vapor Deposition (PECVD) method. Thus, thin films were produced in a pure state and on any desired surface.

Due to the hydrophobic properties of porphyrins, and their tendency to aggregate by stacking of the planar molecules they are difficult to work with in aqueous media (Rabiee

et al., 2019). Polymer thin films obtained by plasma polymerization shows good biocompatibility when compared to classical biomaterials (Yasuda & Gazicki, 1982). The vapor deposition method is a dry technique used to deposit targeted monomer material or materials as a thin film on a desired surface without using any solvents during the film synthesis and polymerization processes within the system (Dianatdar et al., 2023).

Plasma polymerization is a thin film formation process in which thin films are deposited directly onto substrate surfaces without any additional fabrication. In the plasma polymerization process, monomers are converted into polymers with the assistance of plasma, and these polymers deposit as thin films on the substrate surfaces. Therefore, the plasma polymerization process performs both thin film formation and polymerization in a single step, without the use of solvents or chemicals. Plasma generates free radicals on the surface, which initiate polymerization. Consequently, in this process, plasma is considered a radiation source that generates free radicals (Inagaki, 2006; Kulkarni, 2018; Nageswaran et al., 2018). The mechanism of plasma polymerization is shown in Figure 2.9.

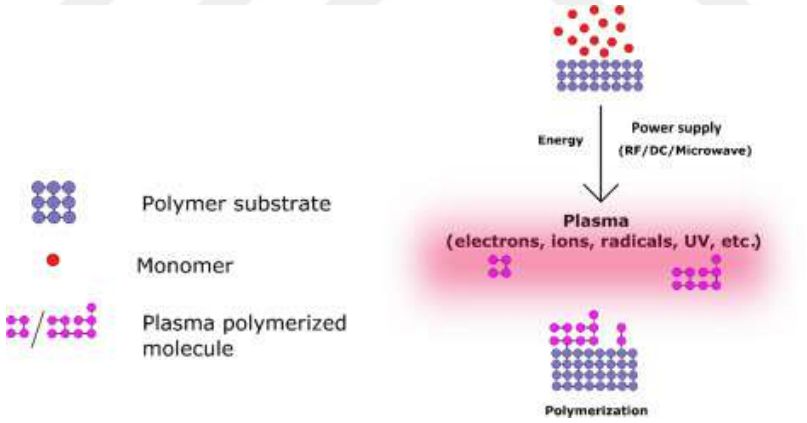

Figure 2.9 Mechanism of plasma polymerization (Nageswaran et al., 2018)

Plasma Enhanced Chemical Vapor Deposition (PECVD) is a vacuum deposition/coating method used to form a thin film layer by activating gas-phase monomers using plasma. Its primary advantage is that reactions are initiated by plasma energy rather than thermal energy. While high temperatures or chemical catalysts are required for the reaction to occur in conventional Chemical Vapor Deposition (CVD) methods, in the PECVD system, gas molecules are ionized by energetic electron bombardment, enabling the

production of high-purity thin films at lower temperatures. This feature positions the method as significant in biomedical applications and the coating of temperature-sensitive, delicate surfaces (Bhushan & Jung, 2011; Campbell, 1996; Carlsson & Martin, 2009). Figure 2.10 shows a photograph of the PECVD system used for the thesis studies.

Figure 2.10 Custom made PECVD system

3. MATERIALS AND METHOD

3.1 Materials

Tetraphenylporphyrin (TPP), pyrrole, and thiophene were purchased from Sigma-Aldrich for use in the synthesis of copolymer thin films and were used without any further purification. Glass slides (ISOLAB) and silicon wafers (SIEGERT WAFER) were used as substrates for the coating processes. The substrates were cleaned using 99% purity chloroform and 70% purity isopropyl alcohol. Plasma polymerization processes were carried out in a custom-built Plasma-Enhanced Chemical Vapor Deposition (PECVD) system (Kenar Mühendislik). This experimental setup consists of a vacuum reactor chamber, an RF plasma source (RFPT Co., Ltd) for monomer activation, and a vacuum pump (Vacuubrand VAP5) to achieve the required pressure levels. In addition, a cold trap (CLS CLCT -40) was integrated into the system to condense chemical vapors during the coating process and to protect the vacuum pump from contamination.

For the structural and optical characterization of the synthesized thin films, in-house spectroscopic analyses were performed using a JASCO 4700 Spectrophotometer for Fourier Transform Infrared (FTIR) spectroscopy and a JASCO V-750 Spectrophotometer for Ultraviolet–Visible (UV–Vis) spectroscopy. Scanning Electron Microscopy (SEM), Atomic Force Microscopy (AFM), and X-ray Photoelectron Spectroscopy (XPS) analyses for surface and morphology characterization were conducted through service procurement from the Middle East Technical University Central Laboratory (METU-MERLAB).

3.2 Method

3.2.1 Simulation studies of thin film synthesis

The initial chemical structures of the copolymers, which were formed from TPP and electron-accepting groups (Thiophene and Pyrrole), were established by taking a 1 to 1 molar ratio of each monomer. The connection points of the monomers forming the copolymer, and subsequently the connection points of the copolymers (again at a 1 to 1 molar ratio), were determined through detailed conformational analyses. Then, molecular modelling of the relevant oligomers was performed based on the obtained comonomers, and the chemical structures of the polymer films to be synthesized experimentally were determined theoretically beforehand. Following this, the absorption spectrum of the polymers with determined chemical structures were simulated using the same quantum mechanical method, and potential shifts predicted to occur in the absorption wavelengths were identified.

In this manner, the relationship between the chemical structure and the absorption wavelength was clearly established theoretically, which guided the experimental studies. The molecular modelling and absorption spectrum studies, performed at the LSDA/6-311G calculation level (a DFT method), were simulated under atmospheric pressure and at room temperature. All calculations were performed using the Gaussian 09 program package.

3.2.2 Sample preparation

Prior to the coating process, silicon and glass substrates were immersed in 70% isopropyl alcohol for 10 minutes for sterilization purposes. Subsequently, the substrates were held by their edges using forceps, and their corners were touched to filter paper to drain the excess alcohol. They were then left to air-dry in a petri dish. Following the drying process, the samples were placed onto the sample holder and secured using Kapton tape.

3.2.3 Determination of copolymer-based thin film synthesis parameters

The synthesis of TPP-co-thiophene and TPP-co-pyrrole thin films using the Plasma-Enhanced Chemical Vapor Deposition method is one of the unique aspects of the thesis and was performed for the first time within this scope. The PECVD process was carried out in a custom-made, domestically produced vacuum chamber (reactor) featuring five inlet ports [for monomers, flow rate-controlled gases, and RF power source] and one outlet leading to the vacuum pump. To prevent peeling/delamination of the synthesized thin films, the substrates placed in the PECVD chamber were first activated with oxygen plasma to facilitate the formation of hydroxyl groups on the surface. The resulting hydroxyl radical groups on the surfaces increased the reactivity of the sample surfaces, allowing them to interact more effectively with the precursors delivered into the reactor.

In the initial stage, coatings were performed for different durations (15, 30, and 60 minutes) at plasma powers ranging from 5 W to 40 W and pressures between 80 and 150 mTorr, without disrupting the structure of the TPP molecules. As the vapors of the monomers were sent into the reactor, the plasma source was turned on at power levels between 5 W and 40 W to activate the molecules and enable their polymerization. In addition to plasma power analyses, the plasma exposure times of the surfaces were also analyzed. The plasma exposure time has the potential to affect the number of radical groups formed on the surface, surface oxidation, and the degree of fragmentation of the precursors (Malik, Rachit, et al., 2013). While short-term plasma interactions were generally required for the activation of sample/substrate surfaces, they could also prevent the attainment of the targeted polymer structure by hindering sufficient fragmentation of the precursor delivered to the system (Chytrosz-Wrobel, Paulina, et al., 2023). For this reason, the effects of 15 min, 30 min, and 1 hour durations on the morphological and chemical structures of the thin films were examined through necessary analyses, and the optimum duration was determined.

3.2.4 Copolymerization and thin film deposition experimental procedure

First, as described in the sample preparation section, glass and silicone substrates were placed in the reactor with Kapton taped sterile sample holder, with the samples facing downwards. To prevent monomers from adhering to the reactor walls as much as possible, the reactor walls and lid were heated to 50 degrees. After placing the chemicals to be used in the experiment into the evaporator or infusion tube, the reactor lid was closed, and the vacuum was activated. When the vacuum level dropped below 120 mTorr, the heaters were activated according to the monomers used. In the experiments, pyrrole and thiophene were evaporated at room temperature, while TPP was evaporated at 315 degrees using an infusion tube. When the desired temperatures and vacuum levels were reached, the plasma source was operated at 5W power, and the monomer valves were opened to increase the vacuum level to the same level. After this process, a timer was set for 1 hour, at the end of the time, the plasma was turned off, and the samples were transferred to a petri dish using forceps.

3.2.5 Characterization methods

In this study, Fourier Transform Infrared Spectroscopy (FTIR), Ultraviolet-Visible Spectroscopy (UV-Vis), Scanning Electron Microscopy (SEM), Atomic Force Microscopy (AFM), and X-ray Photoelectron Spectroscopy (XPS) methods were utilized to understand the chemical, optical, and morphological properties of Polypyrrole (PPy), Polythiophene (PTh), and Tetraphenylporphyrin (TPP) thin films synthesized by the Plasma Enhanced Chemical Vapor Deposition method, as well as TPP-PPy and TPP-PTh thin films synthesized by the polymerization of these monomers.

FTIR was employed to determine the molecular structure of the films and whether functional groups were preserved during plasma polymerization. FTIR analysis is a widely used method to monitor structural changes, particularly the extent to which ring structures are preserved in the plasma environment, the presence of aromatic C-H bonds, and ring fragmentation. Furthermore, it provides information about the polymerization mechanism by comparing the conjugated structures and fingerprint regions of the synthesized polymers with their monomers.

Ultraviolet-Visible Spectroscopy (UV-Vis) analyses were performed to investigate the optical properties of the produced thin films. Especially for porphyrin derivative films, changes in the positions of the characteristic Soret and Q bands offer critical data regarding the conjugation length and PDT efficacy of the film.

SEM and AFM were used to examine the surface morphology, coating homogeneity, and topographic properties of the resulting structures. SEM analyses were preferred to visualize the globular nanostructures typically exhibited by plasma polymers, surface roughness, and film integrity. AFM was utilized for the determination of surface roughness and 3D mapping of topographic details at the nanometer scale. Finally, X-ray Photoelectron Spectroscopy (XPS) analysis was employed to determine the elemental composition and chemical bonding states (oxidation levels, C/N or C/S ratios) on the surface of the films. XPS is a particularly important technique for the depth profile analysis of plasma polymers. This set of analyses aims to verify the suitability of the produced thin films for photodynamic therapy and biomedical applications.

4. RESULTS AND DISCUSSION

4.1 Simulation Studies of Thiophene-co-TPP and Pyrrole-co-TPP Polymers

According to the performed DFT simulation results, while the Soret band of isolated tetrakis appears at 401 nm, it shifted to 468 nm in the comonomer obtained by binding thiophene to tetrakis, to 645 nm in the dimer, and to 655 nm in the trimer. Furthermore, while the Q-band was obtained at 612 nm for tetrakis alone, it underwent a significant shift towards 623 nm in the tetrakis-thiophene monomer and 798 nm in the trimer.

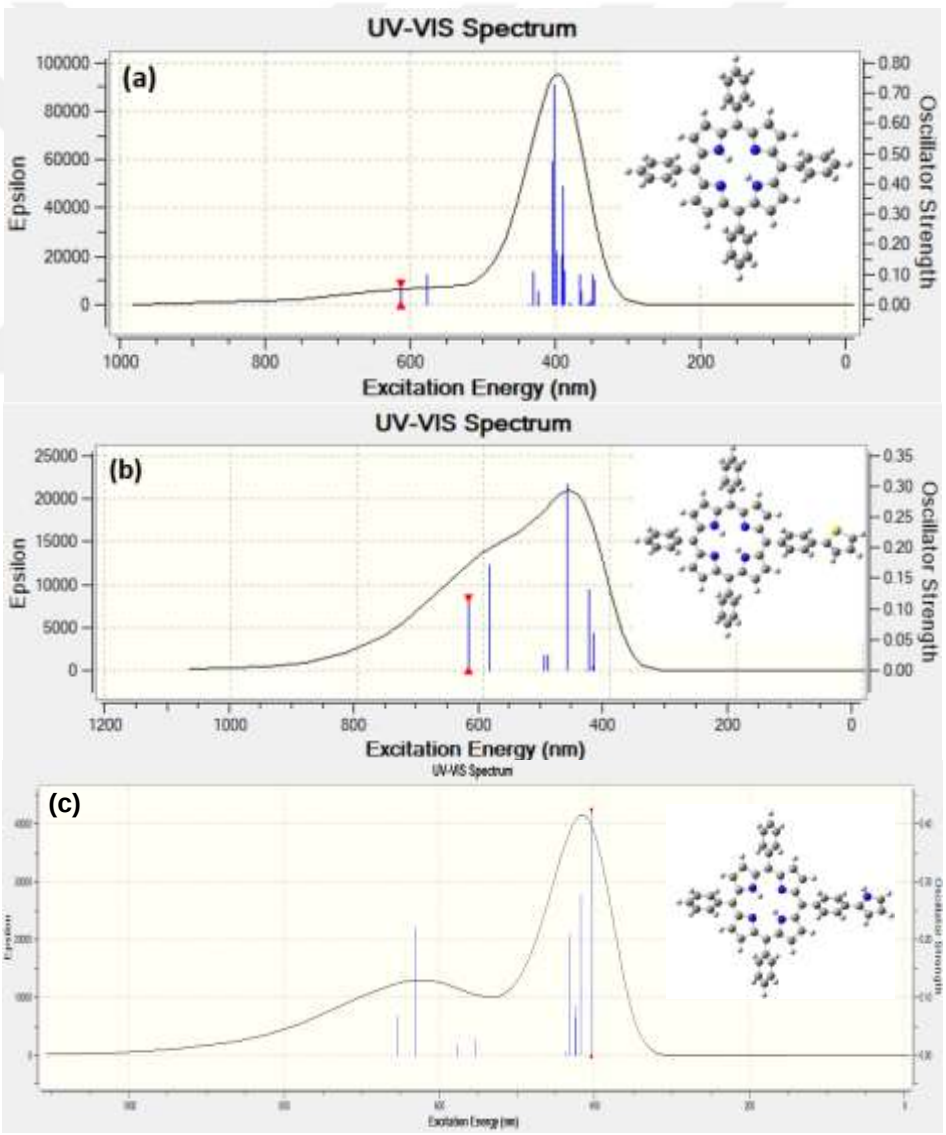

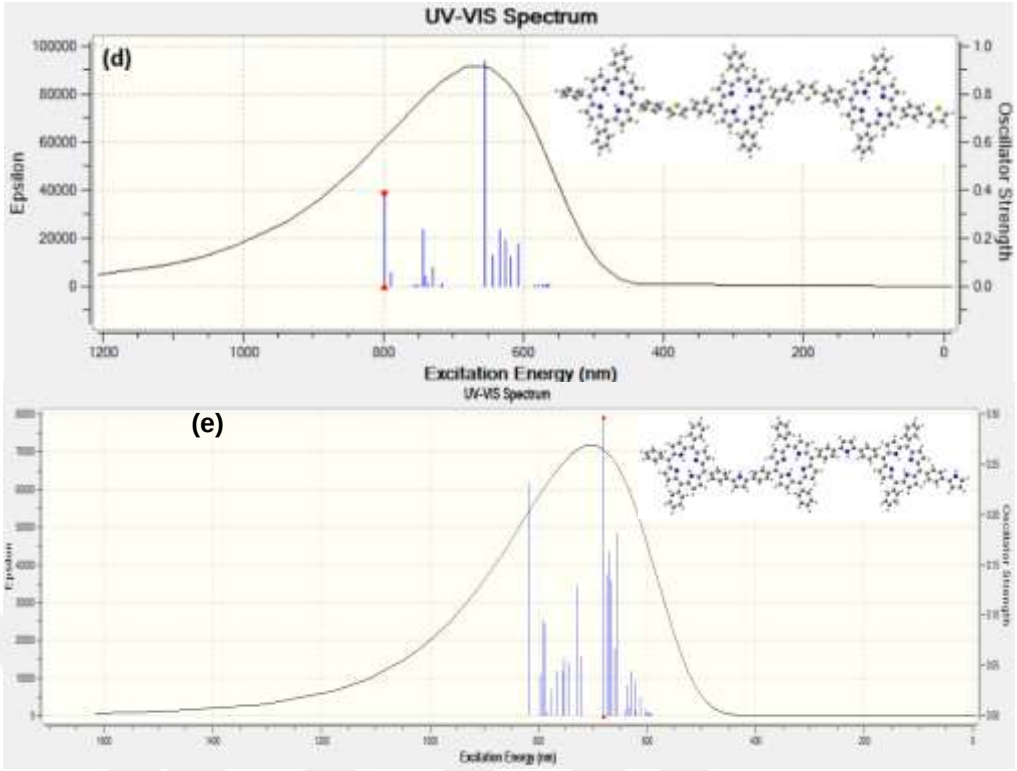

Figure 4.1 Molecular modeling and absorbance spectrum simulations of isolated tetrakis (a), tetrakis-thiophene comonomer (b), tetrakis-pyrrole comonomer (c), tetrakis thiophene trimer (d), tetrakis-pyrrole trimer (e) performed via DFT

For the pyrrole-TPP trimer, the λ_{max} was found to be 680 nm. On one hand, the agreement shown by the Soret and Q-band findings obtained from the experimental absorption spectrum given in Figure 4.1. above and the theoretical spectrum in Figure 4.1.(a) reveals the reliability of the DFT method used; on the other hand, the fact that it shows the shift caused by the copolymerization with thiophene in these two bands demonstrates the importance of using the theoretical approach with DFT in determining the relationship between chemical structure and absorption wavelength.

4.2 FTIR Characterizations

4.2.1 FTIR analysis of polypyrrole thin films

The spectrum image seen in Figure 4.2 is the PPy film on silicon wafers. The spectrum shown in red corresponds to the monomer, while the spectrum shown in green represents the FTIR data of the thin film. The polypyrrole thin film is observed to retain the fundamental structure of the pyrrole monomer. In the FTIR spectrum of the produced PECVD polypyrrole films, the band in the 3250-3340 cm^{-1} range corresponds to the N-H symmetric stretching vibration peaks originating from pyrrole. The peaks observed at 3100 and 3140 correspond to aromatic C-H stretching. The presence of these peaks indicates that, although some of the pyrrole rings have undergone opening by the plasma as will be discussed shortly, the ring form is still preserved within the film. The peaks observed around 2900 are attributed to asymmetric and symmetric C-H stretching vibrations, indicating that the pyrrole has been reorganized under the influence of the plasma (Ahmad et al., 2016; Matsumoto & Honma, 2007; Sakthi Kumar et al., 2003). This phenomenon is an expected situation in plasma polymerizations. The peaks observed at between 2030 and 2160 cm^{-1} indicate cumulative X=Y=Z stretching (where X, Y, Z is C, N, or O) double bonds resulting from plasma-induced fragmentation and reorganization (Goktas et al., 2009). The 2160-2230 cm^{-1} peaks represent triple bond stretching in the literature and indicate that the pyrrole ring structure also exists in an opened form (Iriyama & Wa, 2001; Kravets et al., 2010).

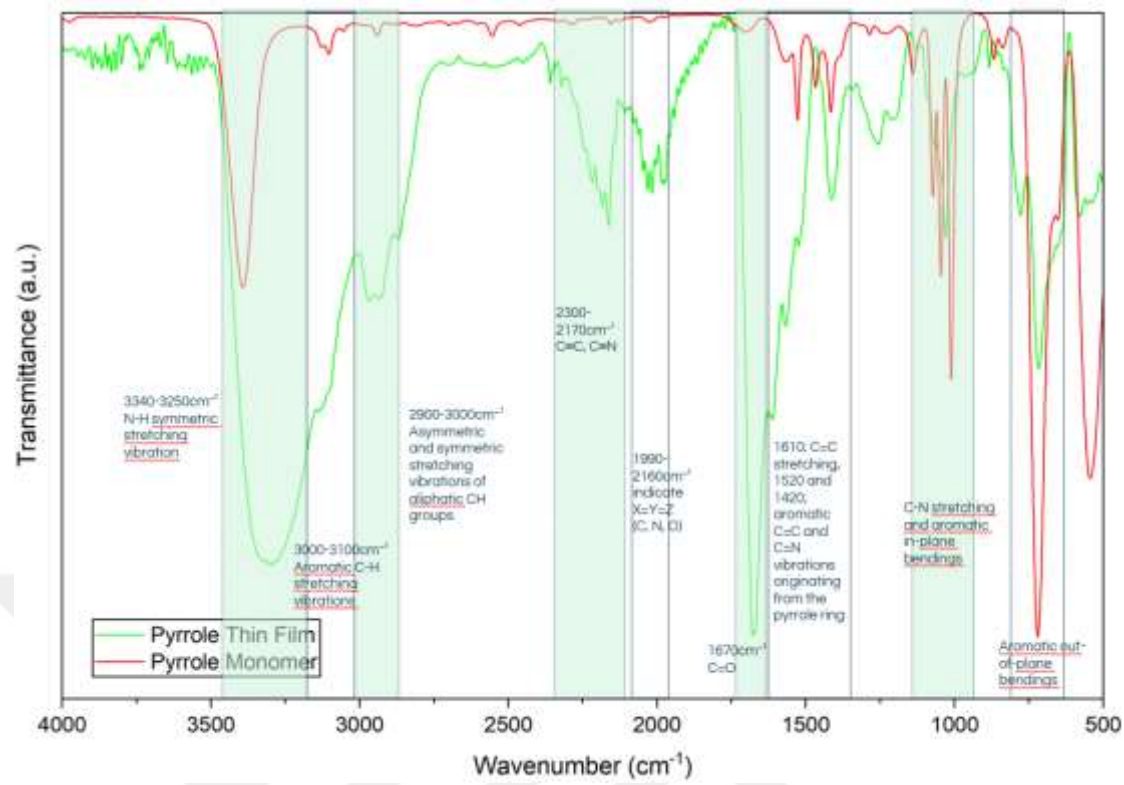

Figure 4.2 FTIR spectrum of polypyrrole thin film

Although 1670 could be assigned to C=C group, it is observed from the XPS results that oxidation has occurred and the intense peak obtained, points to C=O stretching according to Iriyama and Wa. Considering these data, it is concluded that the active radicals trapped within the film reacted with oxygen upon the film's contact with it at the end of the experiment. The peak observed at 1610 indicates C=C stretching bonds, while the peaks seen at 1520 and 1420 indicate aromatic C=C and C=N vibrations originating from the pyrrole ring (Hemant Keshav, 2021; Iriyama & Wa, 2001; Fally et al., 1991). The peak at 1250 cm^{-1} can be attributed to C-N stretching from pristine pyrrole ring (Jang et al., 2023). The observation of these vibration peaks specific to the aromatic ring and stretching peaks from double bonds demonstrates that conjugated polymerization has occurred in the polypyrrole thin film and that the ring structure is largely preserved. Additionally, the aromatic in-plane bending peak observed at 1027 and the C-H aromatic out-of-plane bending peak observed at 715 are among the most important data indicating the ring structure (Ahmad et al., 2016; Ibrahim et al., 2013; Kamal & Bhuiyan, 2013).

4.2.2 FTIR analysis of polythiophene thin films

The spectrum image seen in Figure 4.3 is the PTh film on silicon wafers. The spectrum shown in red corresponds to the monomer, while the spectrum shown in green represents the FTIR data of the thin film. As also observed in the previous section, the polythiophene thin film is observed to retain the fundamental structure of the thiophene monomer. In the produced PECVD polythiophene films, although thiophene does not contain OH groups, the peak observed at 3289 cm^{-1} is attributed to oxidation detected during ex-situ FTIR measurements, a phenomenon reported in the literature for plasma-polymerized thiophene films (Bayram, 2019; Cho & Boo, 2012). The peaks observed at 3022, 3066, and 3100 cm^{-1} indicate aromatic C-H stretching vibrations. The peaks corresponding to 2960 and 2916 cm^{-1} represent the asymmetric and symmetric stretching vibrations of CH_2 groups (Bhat & Wavhal, 1998; Tanaka et al., 1990). These peaks, which are absent in the thiophene monomer, indicate that the structure has undergone fragmentation and rearrangement, as expected in plasma polymerization.

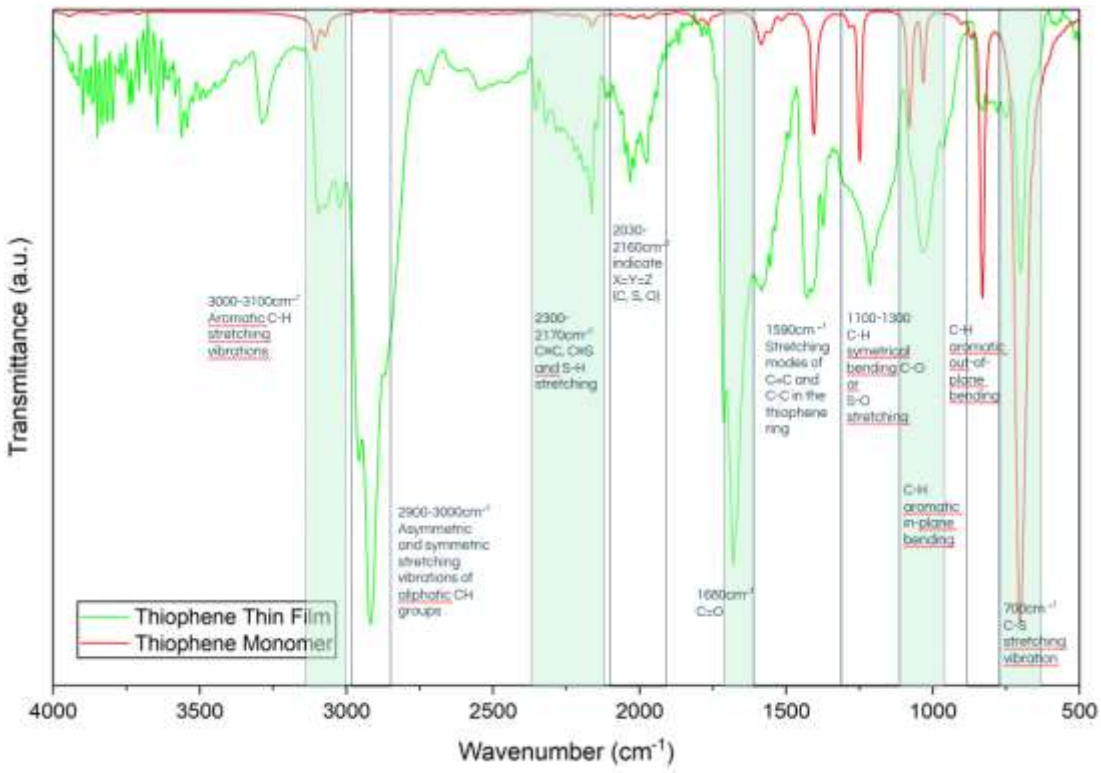

Figure 4.3 FTIR spectrum of polythiophene thin film

The peaks observed at 2030 and 2160 cm^{-1} indicate cumulative X=Y=Z (where X, Y, Z is C, S, or O) double bonds resulting from plasma-induced fragmentation and reorganization (Goktas et al., 2009). The presence of the OH group peak at 3289 cm^{-1} supports the assignment of the intense peak observed at 1680 cm^{-1} to C=O stretching (Cho & Boo, 2012; Tanaka et al., 1990). The peak observed at 1580 cm^{-1} represents the characteristic stretching of conjugated C=C bonds within the thiophene ring and the polymer chain. According to Goktas et al., the peak appearing at 1420 cm^{-1} corresponds to the methylene group bonded to a sulfur atom (CH_2-S) (Goktas et al., 2009). Based on the literature and considering the peaks observed at 3289 and 1680 cm^{-1}, the peak at 1215 cm^{-1} can be attributed to S-O or C-O stretching. The peaks observed at 1030 and 700 cm^{-1} are characteristic peaks of polythiophene and can be attributed to aromatic C-H aromatic out-of-plane bending and C-S stretching vibration originating from polythiophene, respectively (Silverstein & Visoly-Fisher, 2002; Bhat & Wavhal, 1998; Goktas et al., 2009; Groenewoud et al., 2000).

4.2.3 FTIR analysis of pyrrole-co-thiophene copolymer thin films

The broad region observed at 3380–3150 cm^{-1} is the combined appearance of N-H originating from Pyrrole and the OH group observed as a result of free radicals originating from plasma polymerization reacting with oxygen in the environment (Dams et al., 2006; Kamal & Bhuiyan, 2013; Kravets et al., 2010). The 3100-3050 region corresponds to aromatic C-H stretchings originating from pyrrole and thiophene with intact ring structures (J. Zhang et al., 1997a). The 2930 cm^{-1} & 2875 cm^{-1} bands, which are not present in pyrrole and thiophene monomers, indicate aliphatic C-H groups emerging via ring fragmentation (Cho & Boo, 2012; Wang et al., 2004).

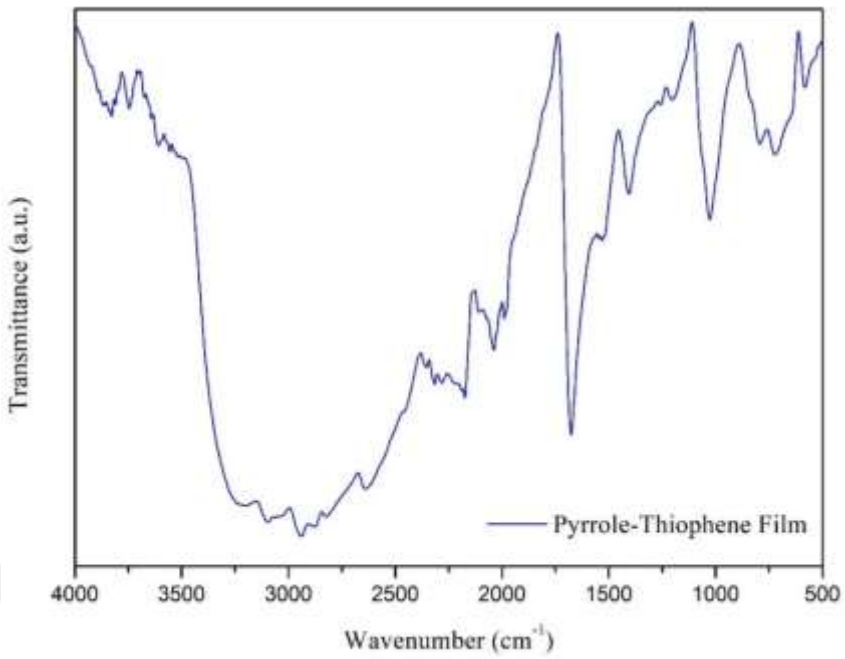

Figure 4.4 FTIR spectrum of pyrrole-co-thiophene thin film

The peaks observed in the 2300-2170 range indicate triple bonds in a typical FTIR spectrum. In this film, they indicate C≡N and C≡C bonds. At the same time, especially in thiophene films, this region indicates C≡S and S-H stretching signals (Wang et al., 2004). The 2100-1990 range is the cumulative double bond (X=Y=Z) region; generally, double bonds of C, H, and O originating from the environment, as well as nitrogen originating from Pyrrole and sulphur originating from thiophene, exist in a complex state (Goktas et al., 2009; Kamal & Bhuiyan, 2013). The intense C=O observed at 1670 and 1680 in thiophene and pyrrole, respectively, manifests itself at 1677 in this film (J. Zhang et al., 1997a). 1530 and 1570 indicate the aromatic C=C bond originating from pyrrole and thiophene, while 1405 indicates the C-N stretching originating from pyrrole. Subsequently, 1025 indicates C-H in-plane bending, 839 C-S stretching, 794 out-of-plane bending, and 720 N-H wagging motion (Bayram, 2019; Liu et al., 2009; Wang et al., 2004). The peak, which manifests itself as a shoulder shaped pattern around 650, indicates C-S stretching vibration (Groenewoud et al., 2000).

4.2.4 FTIR analysis of TPP thin films

Figure 4.5 presents the FTIR spectrum of the TPP thin film. Firstly, the peak observed at 3390 cm^{-1} corresponds to N-H stretching. This indicates that the film retains the pyrrolic core (Dinache et al., 2022; El-Nahass et al., 2005; Şen et al., 2010). Also in Figure 4.5, the 3000-3500 range is shown in a zoomed-in and deconvoluted view. 3250 cm^{-1} may belong to a terminal alkyne or O-H structure formed by ring fragmentation. However, the band seen in 1720 proves the presence of OH in the thin film (Titov et al., 2008). The peak observed at 3095 cm^{-1} indicates the C-H stretching originating from the preserved ring structure. In contrast, the peaks observed at 2872, and 2917 cm^{-1} originate from aliphatic C-H bonds (Makhlouf et al., 2014). When the presence of N-H stretching is combined with the presence of aromatic and aliphatic C-H peaks, it appears that a portion of the porphyrin or phenyl rings has fragmented and converted into open-chain hydrocarbon structures, and that TPP is linked by aliphatic bridges. This result is also consistent with the UV-Vis data.

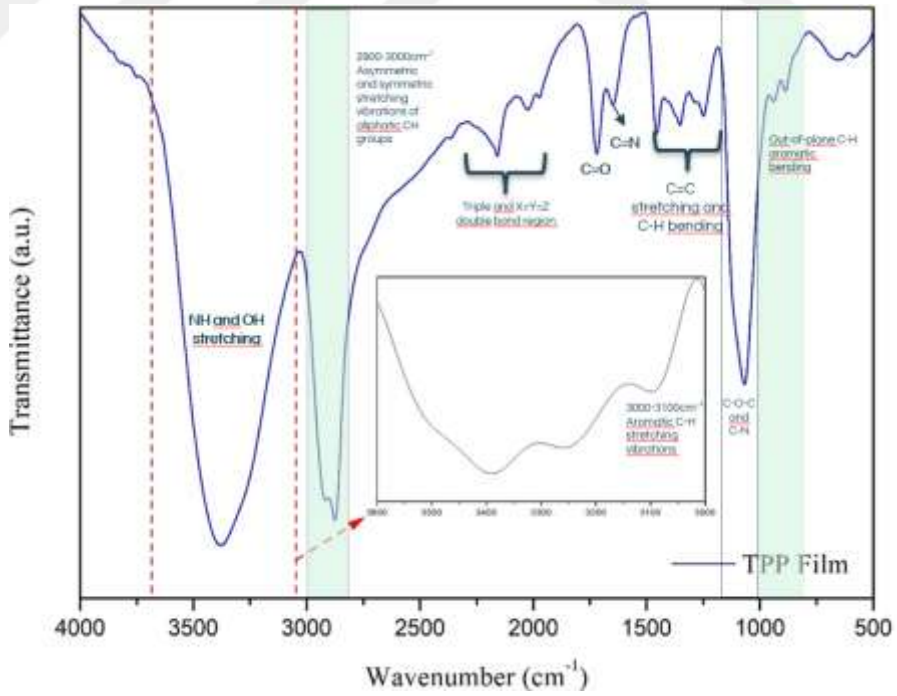

Figure 4.5 FTIR spectrum of TPP thin film. The area between the red dash lines is zoomed in and shown as deconvoluted spectrum

The peak observed at 1720 cm^{-1} is the characteristic C=O peak observed in plasma polymerization (Dinache et al., 2022b; Titov et al., 2008). The broad peak starting from the 3030 cm^{-1} level and extending to 3600 cm^{-1} reinforces the presence of oxygen. 1649 is attributed to N=H vibration (Kravets et al., 2010; Titov et al., 2008). The 1455 peak indicates the aromatic C=C bond, while 1350 cm^{-1} indicates C-C stretching and C-H bending motions (Dinache et al., 2022b; El-Nahass et al., 2005). This peak corresponds to C-O-C ether bridge stretching or C-N/C-H modes. In alkoxy-substituted porphyrins (like hexoxyphenyl TPP), a dominant peak at 1246 cm^{-1} is attributed to C-O-C vibrations. TPP also shows bands in the 1247–1256 cm^{-1} range due to C-H bending and C-N stretching in the porphyrin ring (El-Nahass et al., 2005.; Şen et al., 2010). 1064 cm^{-1}: This matches vibrations for C-H in-plane bending, while the peaks appearing at 933 and 881 indicate aromatic C-H out-of-plane bending (Dinache et al., 2022b; El-Nahass et al., 2005.; Iriyama & Wa, 2001; Wallin et al., 2006; Zhang et al., 1997).

4.2.5 FTIR Analysis of TPP-co-thiophene thin films

In the TPP-co-Thiophene UV-VİS spectrum, the strong peak observed around 3235 cm^{-1} corresponds to the N-H stretching vibration of TPP. However, while this peak appears around 3300 cm^{-1} for pristine TPP, it was observed to shift to 3235 cm^{-1} upon the addition of thiophene. The interaction between the N-H bonds in the porphyrin structure and the sulfur atom in thiophene reduced the force constant of the N-H bond, causing the vibrational frequency to shift from 3300 cm^{-1} to the 3200 cm^{-1} region (Karweik et al., 1976; Meot-Ner et al., 1972). Due to the broadening of the band, it can be suggested that the 3060–3400 cm^{-1} range includes O-H groups in addition to the N-H stretching. The signal observed as a shoulder at 3060 cm^{-1} corresponds to the aromatic C-H stretching. Aliphatic C-H bonds are observed in the 2850–2950 cm^{-1} range. The peaks in the 1980–2050 cm^{-1} region indicate "cumulative double bonds" (X=Y=Z) specific to plasma polymerization, which are absent in the monomer, or cyano/isocyano (C≡N)-like groups formed because of fragmentation. The peak observed at 2150 cm^{-1} corresponds to C≡S and S-H bonds (Cho & Boo, 2012; Dams et al., 2006; Goktas et al., 2009; Wang et al., 2004).

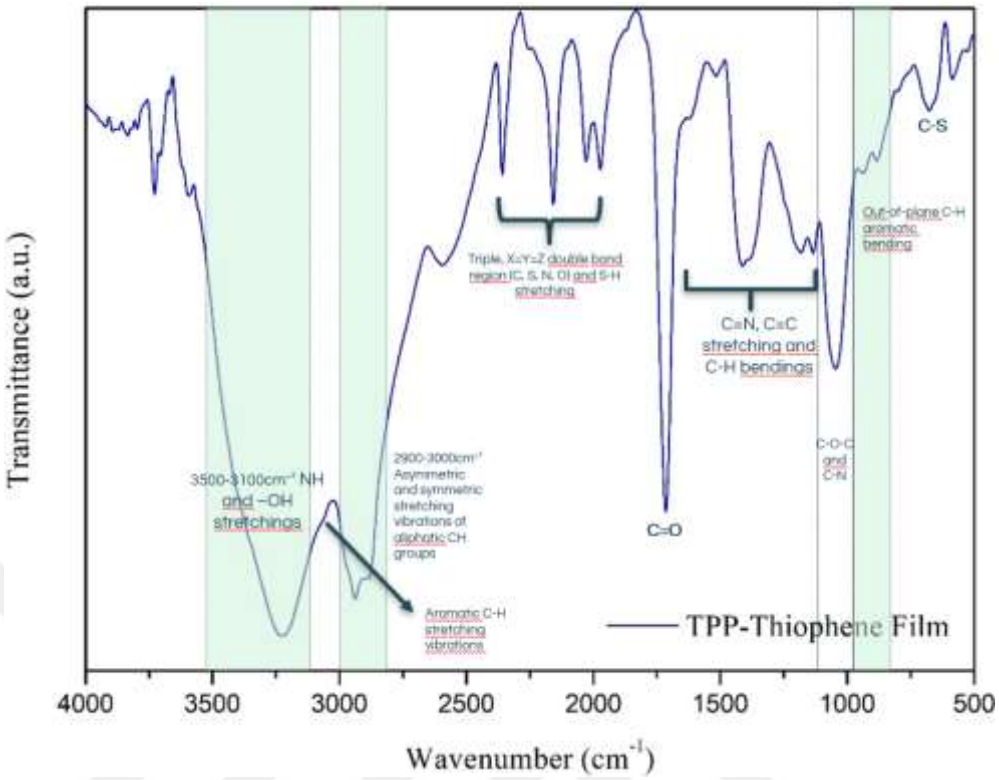

Figure 4.6 FTIR spectrum of TPP-co-thiophene thin film

The peak observed at 670 cm^{-1} is an important indicator of thiophene incorporation. In plasma-polymerized thiophene and oligothiophenes, according to the study by Groenewoud et al. in 2000, the C–S stretching vibration is assigned to the region around 660 (Groenewoud et al., 2000). The peaks in the region between 900 and 1200 indicate C-H out-of-plane and C-H in-plane bending vibrations, respectively. While C–H deformations overlap in this region, bands around 1400–1410 cm^{-1} in thiophene plasma polymers are generally attributed to the C=C stretching specific to the thiophene moiety (Dams et al., 2006). This peak corresponds to C=O stretching (ketones or esters). Since oxygen is not present in the monomers used, this structure is formed as a result of the reaction of long-lived free radicals trapped within the plasma film with atmospheric oxygen and moisture (Cho & Boo, 2012; Dams et al., 2006; Wang et al., 2004).

4.2.6 FTIR analysis of TPP-co-pyrrole thin films

The most critical feature distinguishing thin films produced by plasma polymerization from a simple physical mixture of intact porphyrin and pyrrole is the presence of peaks in the 2000–2250 cm^{-1} region attributed to nitrile (C≡N), isonitrile, or cumulative double bond systems formed by the fragmentation of pyrrole and phenyl rings during plasma polymerization; this situation is also corroborated by Wang et al., Iriyama, and Fally, who describe similar bands resulting from ring breakage in plasma-polymerized pyrrole (Fally et al., 1991; Iriyama & Wa, 2001; Wang et al., 2004). This fragmentation is accompanied by a loss of aromaticity, evidenced by the emergence of strong aliphatic C-H stretching bands in the 2880–2980 cm^{-1} region due to hydrogenation of the carbon skeleton and sp^3 hybridization; this indicates the formation of a disordered, partially saturated network structure that contrasts with the fully aromatic nature of chemically synthesized polypyrrole (Şen et al., 2010; J. Zhang et al., 1997a). Furthermore, the detection of a carbonyl peak at 1677 cm^{-1} points to post-plasma oxidation, where long-lived free radicals trapped within the film react with atmospheric oxygen and moisture to form C=O functional groups; this mechanism is consistent with the observations of Iriyama and Wang regarding radical quenching and nitrile hydrolysis. The bands at 1610, 1560, and 1420 cm^{-1}, corresponding to C=C and C=N stretching vibrations, confirm that while the matrix is heavily cross-linked, it still retains the essential cyclic structures characteristic of plasma-polymerized pyrrole (Iriyama & Wa, 2001; Wang et al., 2004). Although aromatic peaks (3098 cm^{-1}; aromatic C-H bond, 1610 cm^{-1}; aromatic C=C bond) are present, these peaks are shared by both TPP and the pyrrole matrix. There is no distinct evidence that specific TPP core vibrations survive independently.

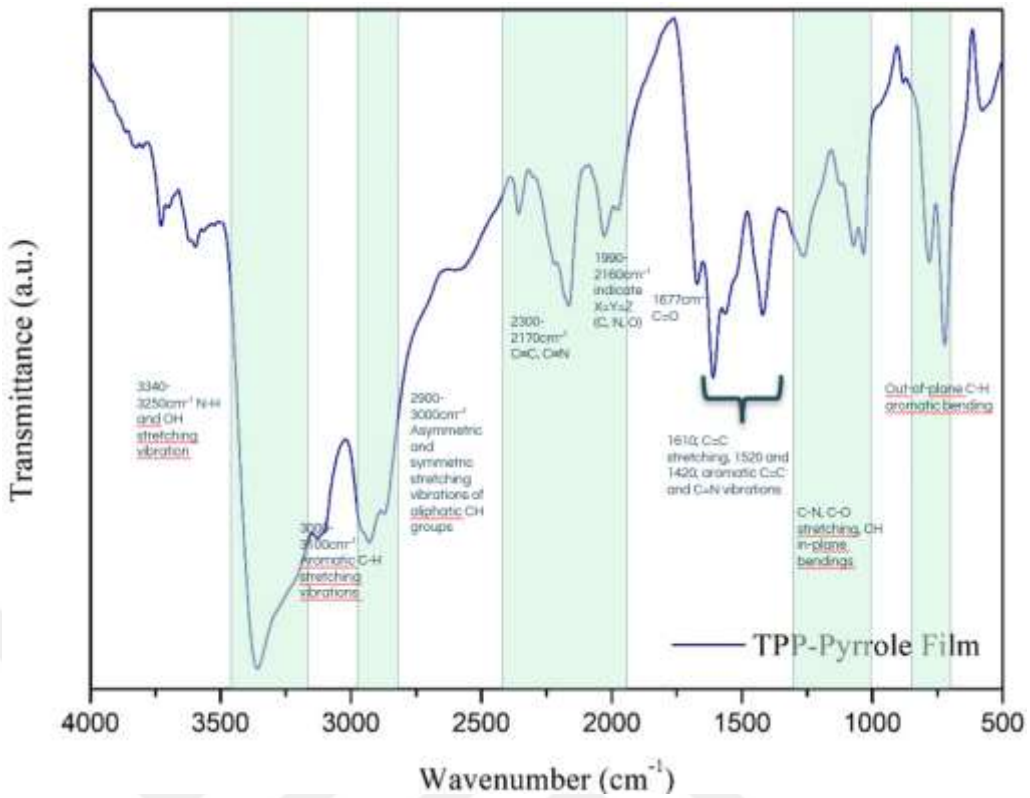

Figure 4.7 FTIR spectrum of TPP-co-pyrrole thin film

Due to TPP being present in the film at a much lower concentration than pyrrole, the fact that the FTIR spectrum of the TPP-Pyrrole thin film shown in Figure 4.7. is almost identical to that of the polypyrrole thin film shown in Figure 4.2, except for the broadening around 3300 due to oxidation and the intensity difference of the C=O peak seen at the 1700 level, also aligns with the UV-Vis data. Therefore, it is thought that TPP is significantly less accumulated in the film due to its molecular weight (and consequent low vapor pressure). During the co-deposition of a heavy, non-volatile macrocycle like TPP (~614 g/mol) and a highly volatile, reactive monomer like pyrrole (~67 g/mol) in a PECVD system, it is a probable reason that the thermodynamics of vaporization and plasma polymerization kinetics create an unfavourable environment for the incorporation of the intact porphyrin chromophore. The absence of TPP peaks in the UV-Vis spectrum can be argued to result from a combination of low TPP partial pressure and the plasma-induced fragmentation of the few TPP molecules that managed to enter the phase, caused by the aggressive polymerization kinetics of pyrrole. This section has also been examined in more detail in the UV-VİS spectrum part.

4.3 UV-Vis Spectroscopy Analysis

4.3.1 UV-Vis spectral analysis of polythiophene thin films

In figure 4.8, the thiophene monomer exhibits a characteristic π-π* transition at a wavelength of 235 nm (Goktas et al., 2009). In the polythiophene thin film, this band shifts to the 330 nm level, indicating that the aromatic structure of thiophene is preserved within the thin film and that the conjugated structure has significantly increased due to the polymerization of thiophene.

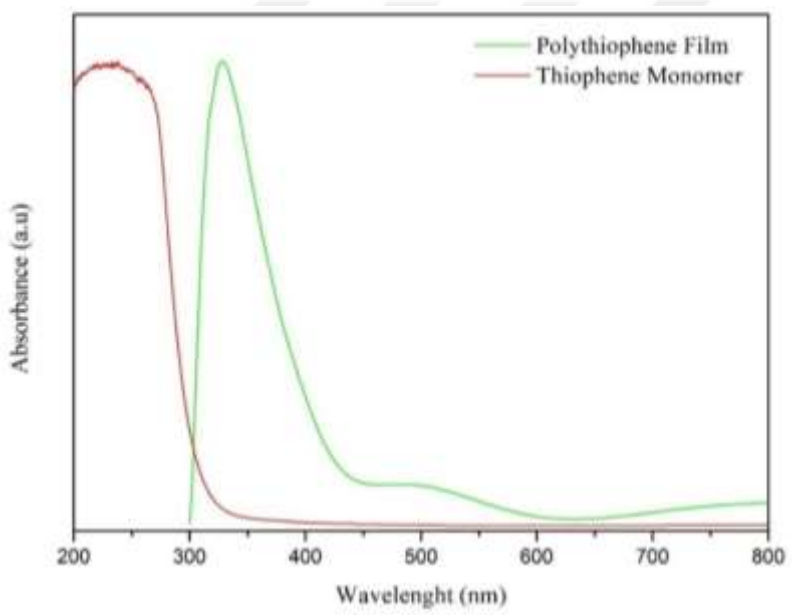

Figure 4.8 Normalized UV-Vis spectrum of thiophene monomer and PTh film

While the thiophene monomer does not exhibit absorption beyond this point, the synthesized thin film displays absorption to around 450 nm, this bathochromic shift demonstrates the conjugated nature of the thin film. The notably broad absorption bands observed around 500 and 800 nm can be attributed to the amorphous film structure resulting from the PECVD process or to alterations in the optical properties of thiophene due to oxidation.

4.3.2 UV-Vis spectral analysis of polypyrrole thin films

In figure 4.9, Pyrrole monomer exhibits the characteristic π-π* transition of pyrrole at 311 nm level and PPy thin film shows an absorbance peak at around 338 nm. Additionally, a red shift of approximately 25 nm is observed in the absorption character of PPy across the spectrum. The absorption spectrum of the PTh thin film, extending up to 600 nm, is indicative of the film's long-chain structure. Both UV-Vis and FTIR data demonstrate that while the aromatic structure is largely preserved in the pyrrole experiments following PECVD.

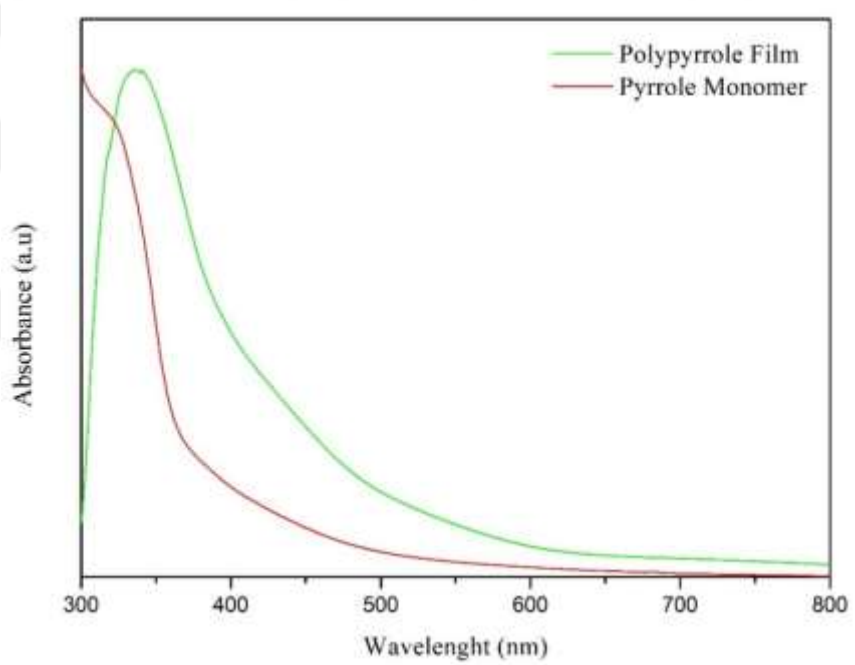

Figure 4.9 Normalized UV-Vis spectrum of pyrrole monomer and polypyrrole film

4.3.3 UV-Vis spectral analysis of pyrrole-thiophene copolymer thin films

The UV-Vis absorption spectrum of the pyrrole-thiophene copolymer film exhibits a maximum intensity around 331 nm and a tailing effect extending to 575 nm, virtually identical to the spectrum of the pyrrole thin film. The intense absorption of the dark brown pyrrole matrix across the visible region likely masks the weaker absorption bands of the yellow-transparent thiophene film (Al-Hamdan et al., 2022; Tan & Ghandi, 2013).

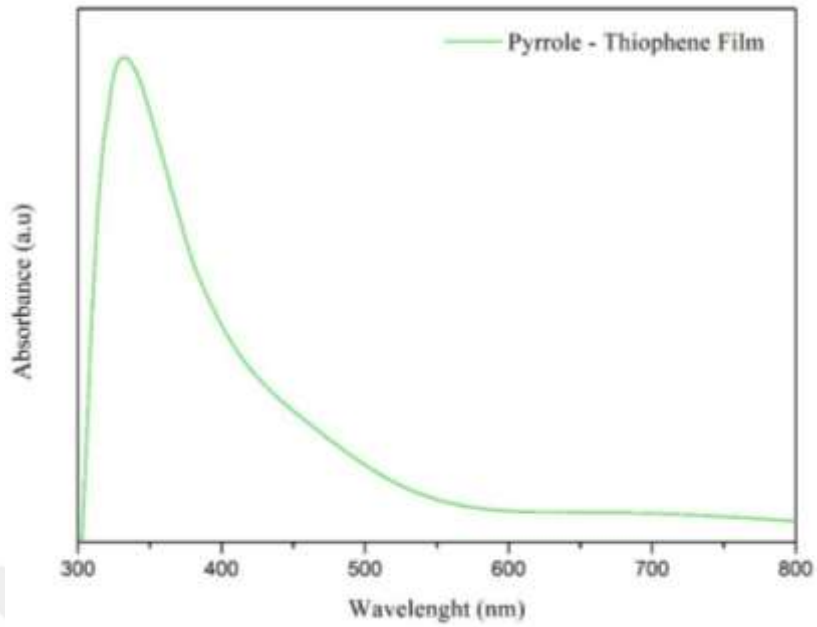

Figure 4.10 UV-Vis spectrum of pyrrole-thiophene copolymer thin film

4.3.4 UV-Vis spectral analysis of TPP thin films

Figure 4.11 displays the UV-Vis absorption spectrum of the TPP monomer and the TPP thin film. The characteristic band observed at 411 nm for the monomer and around 433 nm for the thin film is known as the Soret band, which originates from the π–π* transitions of porphyrins. The 20 nm red shift observed in the Soret band clearly indicates an increase in conjugation. This trend persists across the four weak Q bands as well with 514→520, 549 →554, 589 →594 and most importantly 645 →650 nm.

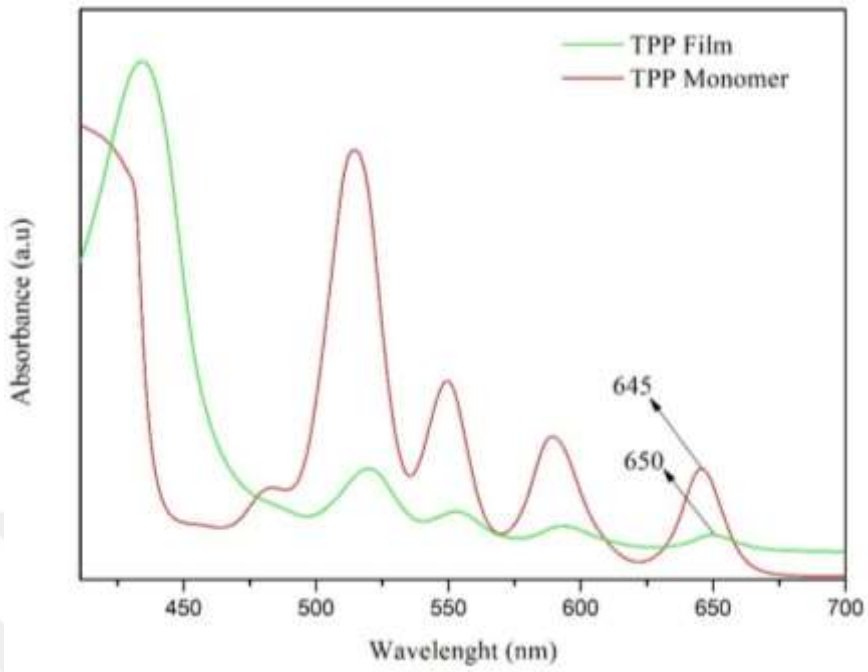

Figure 4.11 Normalized UV-Vis spectrum of TPP monomer and TPP film

The four peaks observed in the spectrum following the Soret band correspond to the Q1y, Q0y, Q1x, and Q0x bands as shown in Figure 4.12 for porphyrins. The Q0 band arises from the electronic transition between the ground state and the first electronic state, whereas the Q1 band involves molecular vibrations in addition to the electronic transition. The x and y subscripts show the polarization of the electric vector of the absorbed light.

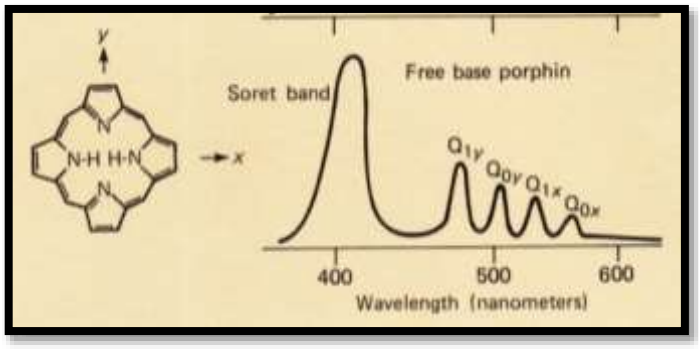

Figure 4.12 Visualization of absorption bands in free base porphyrins (B. F. Kim & Bohandy, 1981)

In a study conducted by Shoji and colleagues in 2007 using plasma polymerization, it was shown that films produced without plasma, using only vapor deposition, that is, without the polymerization stage, dissolved in commonly used organic solvents, whereas thin films produced using plasma did not dissolve (Shoji et al., 2007). For this reason, in order to gain insight into the structure of the plasma-produced TPP thin film, the film was immersed in isopropyl alcohol for 5 minutes. Consequently, UV-Vis characterization was performed again, and the same result was obtained. Therefore, it was understood that a cross-linked polymer film was formed on the surface and that the 5 nm red shift was not caused by the stacking of monomers adsorbed on the surface without polymerization.

The insolubility of the film is definitive proof that the molecules are linked to each other by covalent bonds (Touloupas et al., 2023; Yasuda, 2005). The attachment of porphyrin units to each other via covalent bonds oligomerization expands the interaction area of the π-electron system. This reduces the energy gap and has caused the 5 nm shift in absorption. Additionally, in a study conducted in 2002, it was stated that in porphyrin-based oligomeric structures, face-to-face dimers cause a blue shift in absorption bands, whereas head-to-tail dimers cause a red shift (Aratani et al., 2002). However, since only a 5 nm shift is observed, it is thought that the resulting structure is neither a long-chain polymer structure nor a stacking of monomers, but rather a cross-linked, short-chain, amorphous, J-aggregated, oligomeric structure, as expected from plasma polymerization (Villari et al., 2012).

4.3.5 UV-Vis spectral analysis of TPP-co-thiophene thin films

Figure 4.13 shows the UV-Vis spectrum of the TPP-Thiophene thin film. While a 5 nm shift was observed in the Soret and Q bands in the plasma film synthesized solely with TPP, a 10 nm red shift was observed in all bands in the plasma film synthesized together with thiophene. This indicates both that the film produced using only TPP is not merely a result of vapor deposition and that conjugation within the film increased with the addition of thiophene. Furthermore, a significant absorption is observed between the Soret and Q bands compared to the film produced with only TPP.

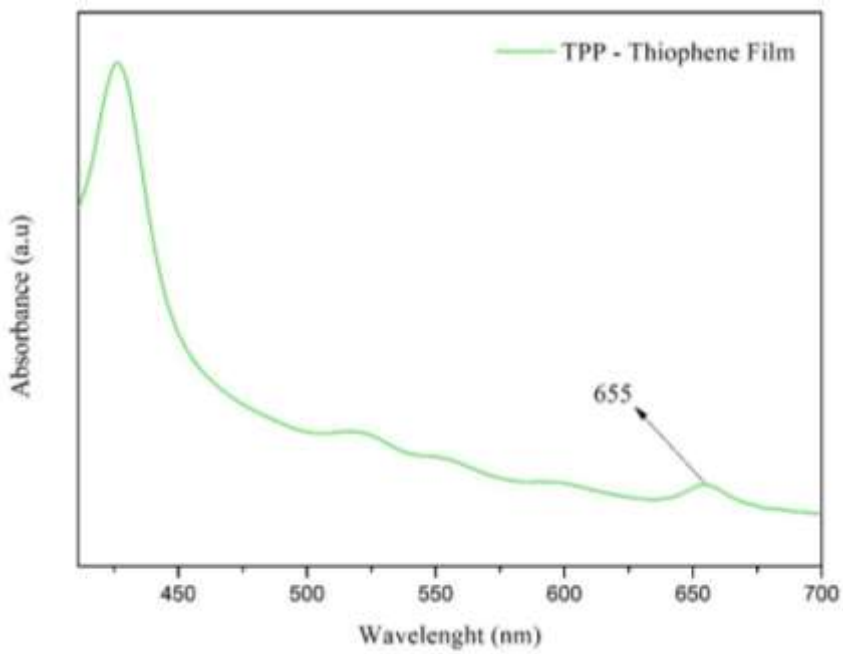

Figure 4.13 UV-Vis spectrum of TPP-co-thiophene copolymer thin film

In a study conducted by Wallin and colleagues in 2006, it is stated that when porphyrins are linked by oligothiophene bridges, the Soret band broadens and the Q bands shift to lower energy (red), and this finding overlaps perfectly with the data obtained in this study (Wallin et al., 2006). Unlike the linear chain porphyrin-thiophene dimer structure produced by Odobel, 2002, via chemical methods, multiple cross-linked structures can form within the film in the chaotic radical environment generated in plasma polymerization. Although the 20 nm shift in the Soret band, the Q1y, Q0y, Q1x bands, and the Q0x band shifting to 655 nm point to an oligomeric structure with increased conjugation (as discussed in the UV-Vis spectrum of the film synthesized using only TPP) the broadening bands and the long absorption structure extending from the Soret band to 700 nm indicate that the film does not strictly contain only TPP-Thiophene-TPP structure formed by thiophene bridges, but also possesses an amorphous structure formed by extensive fragmentation and recombination. (Odobel et al., 2002).

4.3.6 UV-Vis spectral analysis of TPP-co-pyrrole thin films

Figure 4.14 displays the UV-Vis spectrum of the TPP-Pyrrole film. In contrast to the TPP-Thiophene film, the Q bands expected from TPP are not observed in this experiment conducted with pyrrole. Furthermore, as seen in Section 4.3.2, the resulting structure overlaps perfectly with the pyrrole thin film produced solely with pyrrole. The same situation was observed and discussed in Section 4.3.3 regarding the thiophene-pyrrole thin film.

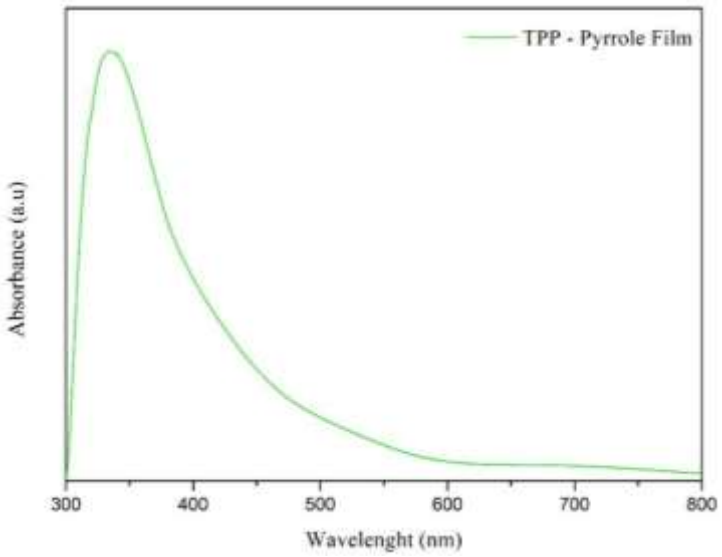

Figure 4.14 UV-Vis spectrum of TPP-co-pyrrole thin film

When examining all UV-Vis characterizations obtained in this study, the film thickness of TPP is also significantly lower compared to Pyrrole under identical conditions. The fact that the molecular weight of TPP is ~614 g/mol while that of Pyrrole is ~67.09 g/mol may have caused the gas-phase concentration of TPP to remain very low relative to pyrrole (which is a volatile liquid, meanwhile TPP is being sublimated at 320 °C under vacuum.) in a mixed plasma such as TPP-Pyrrole (El-Nahass et al., 2005). Additionally, its high reactivity may have led to much faster accumulation on the sample surface, thereby causing TPP to remain at a concentration too low to exhibit its characteristic optical properties (Cruz et al., 1999). Another reason could be the fragmentation of TPP into pyrrole rings in the plasma environment, thus rendering it indistinguishable from the

pyrrole thin film. However, the fact that TPP did not fragment in the plasma environment with thiophene, which is structurally similar to pyrrole, but less reactive, indicates that this situation stems not from fragmentation, but rather from pyrrole depositing much more rapidly and masking TPP.

4.4 X-ray Photoelectron Spectroscopy Characterizations

4.4.1 XPS analysis of thiophene and TPP-co-thiophene thin films

Figure 4.15 presents the XPS spectrum of the thiophene and TPP-co-thiophene thin films produced. The high-resolution and deconvoluted PTh C1s and TPP-co-thiophene C1s spectrum are shown in panels (a) and (d), respectively. Examination of the spectrum shows that in both films the C=C bond appears at 284.3 eV, while the C-C bond is observed at 284.9 eV and 285 eV, respectively (Sahin, 2015; Song et al., 2025). Although the binding energies appear at similar levels, the intensity of the C=C bond increases slightly when thiophene is polymerized with TPP. The peak observed at 285.6 and 285.7 in Thiophene and TPP-co-thiophene films corresponds to C-S, C-N and C-O peaks. While this peak corresponds to C-S in the thiophene thin film, in the copolymer it merges with the C-N originating from TPP, and its area increases by 10%. The reason this increase is lower than expected is that, since both thiophene and pyrrole can volatilize even at room temperature under vacuum, they deposit as a thin film much faster than the sublimation of TPP, which is a much heavier molecule.

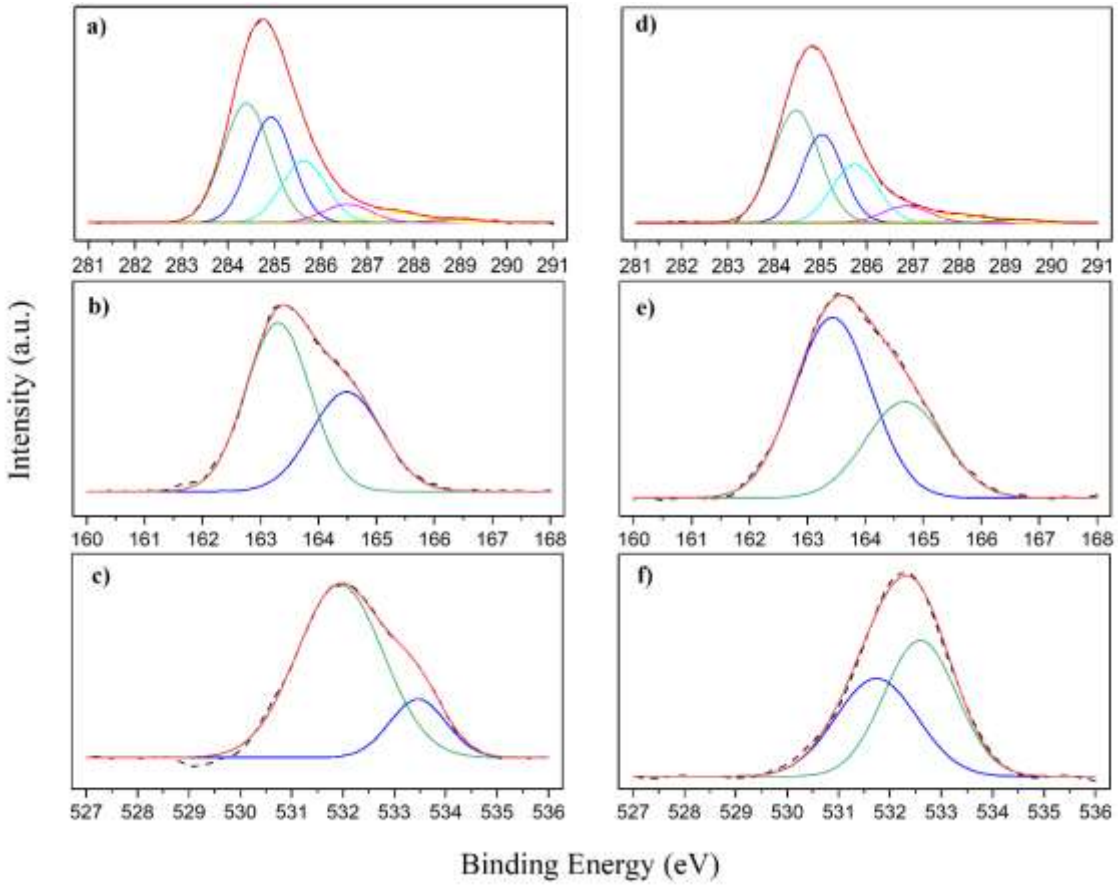

Figure 4.15 High-resolution deconvoluted XPS spectrum of the thiophene thin film and the TPP–thiophene thin film. For the thiophene thin film, a) C1s, b) S2p, and c) O1s; for the TPP-co-thiophene thin film, d) C1s, e) S2p, and f) O1s spectrums are shown

The peaks observed at 286.5 and beyond correspond to groups such as, -C=O, O=C-O, and C=N originating from oxidation; however, due to the low intensity, tail-like appearance, and the area being quite broad, it is not possible to make a precise distinction. In the XPS analysis of the thin film prepared solely with TPP, the nitrogen concentration was found to be 3%, and the N1s region was lost within the noise of the spectrum. The nitrogen content, which is already low due to the molecular composition of TPP ($C_{44}H_{30}N_4$), is further reduced in the film because of the incorporation of thiophene and plasma-induced oxidation introducing oxygen into the system. In addition, considering the sublimation rate of the relatively heavy TPP molecule and the deposition rate of thiophene, which can evaporate even at room temperature, on the silicon wafer, it is understandable that nitrogen becomes indistinguishable from the noise in a surface-sensitive technique such as XPS, which characterizes only the top ~10 nm of the film.

However, the FTIR and UV-Vis analyses, confirm that TPP is present within the film in a state of enhanced conjugation.

Figure 4.15 (b) and (e) show the S2p spectrum of the thiophene thin film and the TPP-co-thiophene thin film, respectively. The S2p spectrum of both films appear identical. The S2p peak corresponding to the PTh film was also deconvoluted into two components, attributed to $S2p_{3/2}$ at 163.3 eV and $S2p_{1/2}$ at 164.5 eV. The doublet structure, originating from spin–orbit splitting and exhibiting an energy separation of approximately 1.2 eV, in which the higher-energy signal has roughly half the intensity of the lower-energy one, corresponds to the S–C bond and is a characteristic feature of thiophene (Teslaru et al., 2016; Vassallo et al., 2007). Figure 4.15 (c) and (f) show the O1s spectrum of the thiophene thin film and the TPP-co-thiophene thin film, respectively. The O1s signals in the range of 531.8–533.5 eV indicate bonds formed because of radical species trapped in the film due to plasma polymerization reacting with atmospheric oxygen and/or moisture. In both films, the lower binding energy signal corresponds to organic surface contamination (carbonyl groups) and hydroxyl groups. The higher binding energy signal, which is observed with higher intensity in the film synthesized with TPP compared to the film synthesized only with thiophene, corresponds to C–O–C bonds (Groenewoud et al., 2003; K. J. Kim et al., 2001; Van Ooij et al., 1996). Since the difference in intensity of the C=O and C–O–C bonds observed between the two films in this spectrum is also observed in the pyrrole thin film and the TPP-co-pyrrole thin film in the same manner, this issue will be discussed in the next section.

4.4.2 XPS analysis of pyrrole and TPP-co-pyrrole thin films

Figure 4.16 presents the XPS spectrum of the pyrrole and TPP-co-pyrrole thin films produced. The high-resolution and deconvoluted PPy C1s and TPP-co-Pyrrole C1s spectrum are shown in panels (a) and (d), respectively. “Since the PP-Py films have most likely a great variety of functional groups present, the curve-fitted peaks are quite broad. Therefore, an exact assignment for the curve-fitted peaks is impossible and only general statements can be made for these films.”(Van Ooij et al., 1996). The regions observed at 284.3 and 285 eV in the pyrrole and TPP–pyrrole spectrum, respectively, correspond to C=C bonds and C-C bonds, while the regions at 285.8 and 285.5 eV correspond to C–N bonds. When the intensity differences between these peaks are considered, the relationship between Figures 4.16 (a) and (d) appears to be highly similar to that between Figures 4.15 (a) and (d). The decrease in the area of the peak corresponding to the C-C structure in the copolymer film compared to the pyrrole thin film, and the increase of the C=C bond structure in the XPS spectrum, again compared to the pyrrole thin film, indicates that conjugated TPP molecules bind into the film, increasing the conjugated bond structure. In agreement with the FTIR spectrum of both films, the C=N bond is present in both of the films. The peaks observed at 286.8 for PPy and 281.1 for TPP-PPy correspond to C=N and C-O groups. The reason this peak appears at lower energy in TPP is that, unlike Pyrrole, the C=N group is also present in TPP itself, leading to an increased concentration. Additionally, the lower oxygen concentration in the copolymer films explains the energy difference between the two peaks. For pyrrole and TPP–pyrrole, the peaks at 287.8 and 287.2 eV represent groups such as C=O, N-C-O and N-C=O.

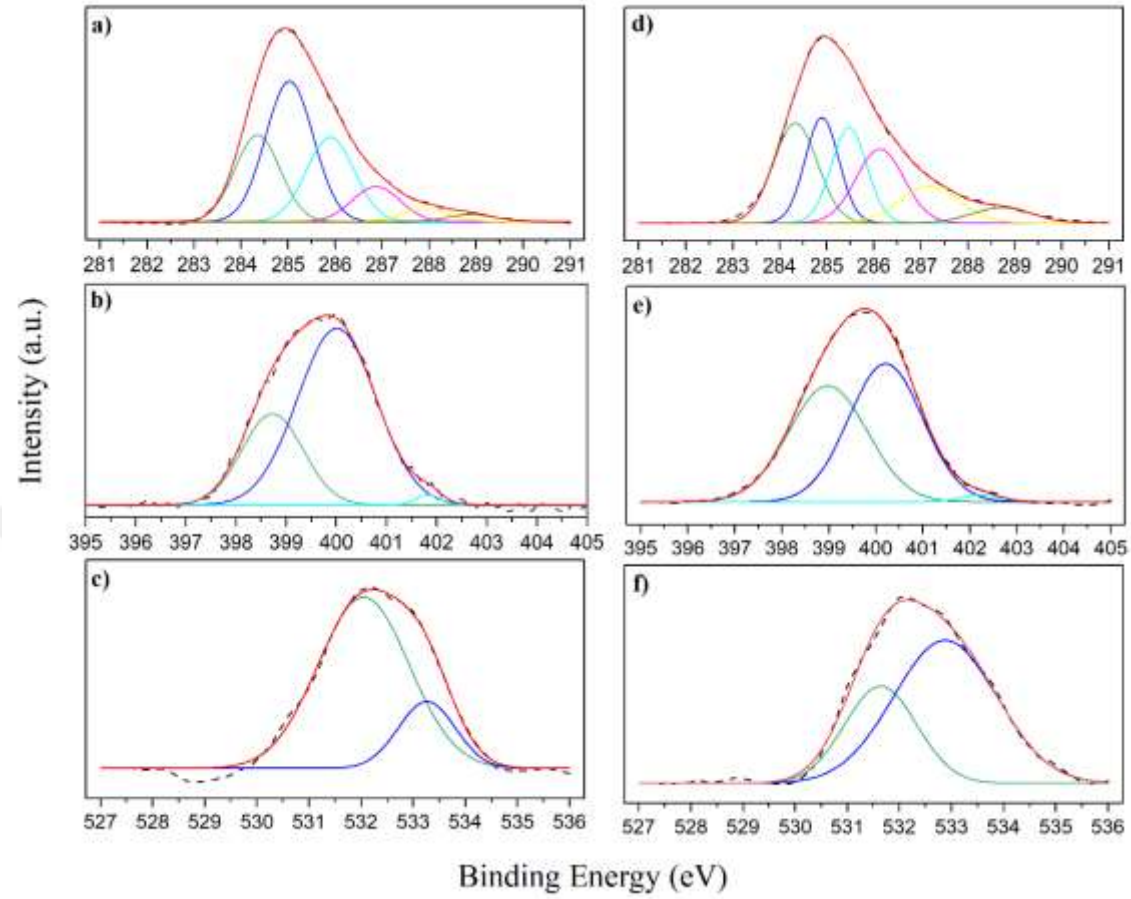

Figure 4.16 High-resolution deconvoluted XPS spectrum of the pyrrole thin film and the TPP-co-pyrrole thin film. For the pyrrole thin film, a) C1s, b) N1s, and c) O1s; for the TPP–Pyrrole thin film, d) C1s, e) N1s, and f) O1s spectrums are shown

Figure 4.16 (b) and (e) show the N1s spectrum of the pyrrole thin film and the TPP-co-pyrrole thin film, respectively. For the pyrrole and TPP-co-pyrrole thin films, the peak at 398.8 eV corresponds to iminic (=N–) nitrogen bonds, while the more intense peaks observed at 400.1 and 400.2 eV correspond to aminic (–NH–) aromatic nitrogen bonds, respectively (Ryan et al., 2020). While =N- is not present in the pyrrole monomer, it is found in its thin film; this is due to fragmentation, but the higher presence of the -NH- group indicates the preservation of the aromatic structure. On the other hand, the =N- group has more area in the copolymer made with TPP, because both the iminic nitrogen structure resulting from fragmentation and =N- group originating from TPP itself appear in the same region. For both films, the broad peak observed around 402 eV, although difficult to assign definitively, corresponds in the literature to positively charged nitrogen

species commonly reported in plasma-polymerized pyrrole-based films (Gomez et al., 2014; Wang et al., 2004; J. Zhang et al., 1997b).

Figure 4.16 (c) and (f) show the O1s spectrum of the pyrrole thin film and the TPP-co-pyrrole thin film, respectively. The O1s XPS spectrum of the pyrrole–TPP and thiophene–TPP copolymer thin films are observed to largely overlap with each other. Similarly, no significant difference is observed between the O1s spectrum of the pristine pyrrole and pristine thiophene thin films. However, when the pristine monomer films (pyrrole and thiophene) are compared with the copolymer thin films formed with TPP, a common and systematic difference emerges for both systems. Although two distinct peaks are detected in all O1s spectrum, the peak at lower binding energy exhibits higher intensity in the pristine pyrrole and thiophene thin films, whereas this distribution is reversed in the TPP-containing copolymer thin films, with the higher binding energy peak becoming dominant. These results indicate that the incorporation of TPP into the copolymer structure leads to a modification of the chemical environment of oxygen and demonstrates a reorganization of the bonding states of oxygen-containing functional groups. Formation of C=O bonds require ring opening, whereas this process is less pronounced when TPP is incorporated into the film matrix. In this system, where conjugation is more extensive, atmospheric oxygen may preferentially form C–O–C bridges rather than C=O bonds, due to the lower extent of ring fragmentation.

4.4.3 Comparative XPS analysis of thiophene-co-pyrrole thin film

Three main components were observed in the C1s spectrum for all (PTh, PPy, Pyrrole-Thiophene) films. The peak with the lowest binding energy was positioned at 284.3 eV for the thin film, which is the aromatic C=C bound from thiophene and pyrrole rings. The second C1s signal observed in the range of approximately 284.9 eV corresponds to C–C bonds, as also discussed in the XPS investigations of thiophene and pyrrole films. The third C1s component observed at higher binding energy (285.6 eV) was attributed to carbon atoms bonded to heteroatoms. While this peak represents C–N bonds for pyrrole and C–S bonds for thiophene, a structure containing the contribution of both bond types

is present in the copolymer film (Atanasoska et al., 1992; Bennettand et al., 1993; Hasik et al., 2002; Z. Zhang et al., 2011).

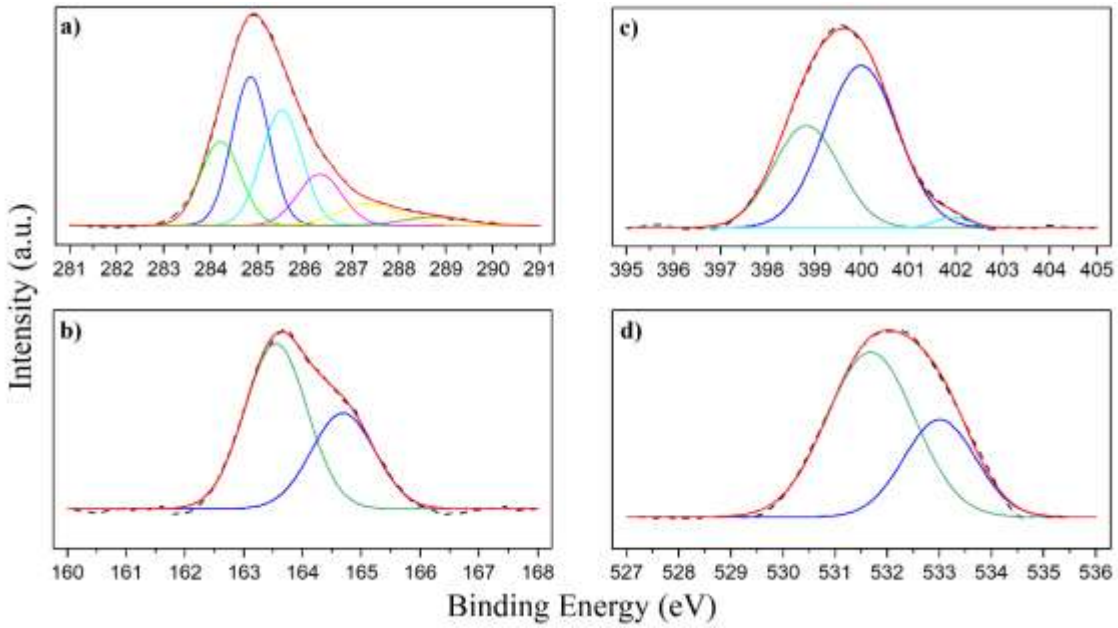

Figure 4.17 High-resolution deconvoluted XPS spectrum of the pyrrole-co-thiophene thin film. The spectrum of C1s, S2p, N1s, and O1s are shown for (a), (b), (c), and (d), respectively

The reason this peak is more intense and broader in the thiophene-co-pyrrole thin film compared to the other films may be due to the introduction of two different molecules into the plasma environment, resulting in a higher abundance of bonds with different structures compared to the other films. In other words, structures such as C–N, C–S, and C–O in the medium appear to be gathered under a single peak (Van Ooij et al., 1996). The N1s, S2p, and O1s spectrum largely overlap with those of the thiophene and pyrrole thin films. No significant difference was found other than the alteration of the charge distribution in the structure caused by the electronegativity properties of nitrogen and sulfur atoms. Comparative XPS data for the Thiophene thin film, Pyrrole thin film, and Thiophene-co-pyrrole thin films are given in Table 4.1.

Table 4.1 Comparative XPS data set of pyrrole, thiophene, and pyrrole-thiophene copolymer thin films

Orbital	Pyrrole Thin Film (eV)	Thiophene Thin Film (eV)	Pyrrole–Thiophene Copolymer Thin Film (eV)	Chemical Bond Assignment
C 1S	284.3	284.3	284.3	C=C
C 1S	285	284.9	284.9	C–C
C 1S	285.8	285.6	285.6	C–S / C–N (heteroatom bonds)
N 1S	398.8	–	398.8	=N– (imine nitrogen)
N 1S	400.1	–	400.0	–NH– (amine nitrogen)
N 1S	401.1	–	401.9	$–N^+$ (positively charged nitrogen)
S 2P	–	163.3	163.5	S $2p_{3/2}$ (C–S–C)
S 2P	–	164.4	164.7	S $2p_{1/2}$ (spin–orbit splitting)
O 1S	532.2	532.0	531.6	C=O (carbonyl)
O 1S	533.2	533.5	533.0	C-O–C (ether)

4.5 Depth Profile Analysis of Thin Films

The depth analysis results indicate that a common feature of the produced thin films is that the oxygen concentration decreases from the surface downwards. This situation explains the presence of oxygen groups observed in the FTIR and XPS results, showing that they are located predominantly on the surface rather than throughout the entire film. Furthermore, for the TPP-co-thiophene thin film, it is understood that the concentration of nitrogen, which was lost within the noise in the XPS data, increases with depth, as seen in the depth analyses in Figure 4.18(c).

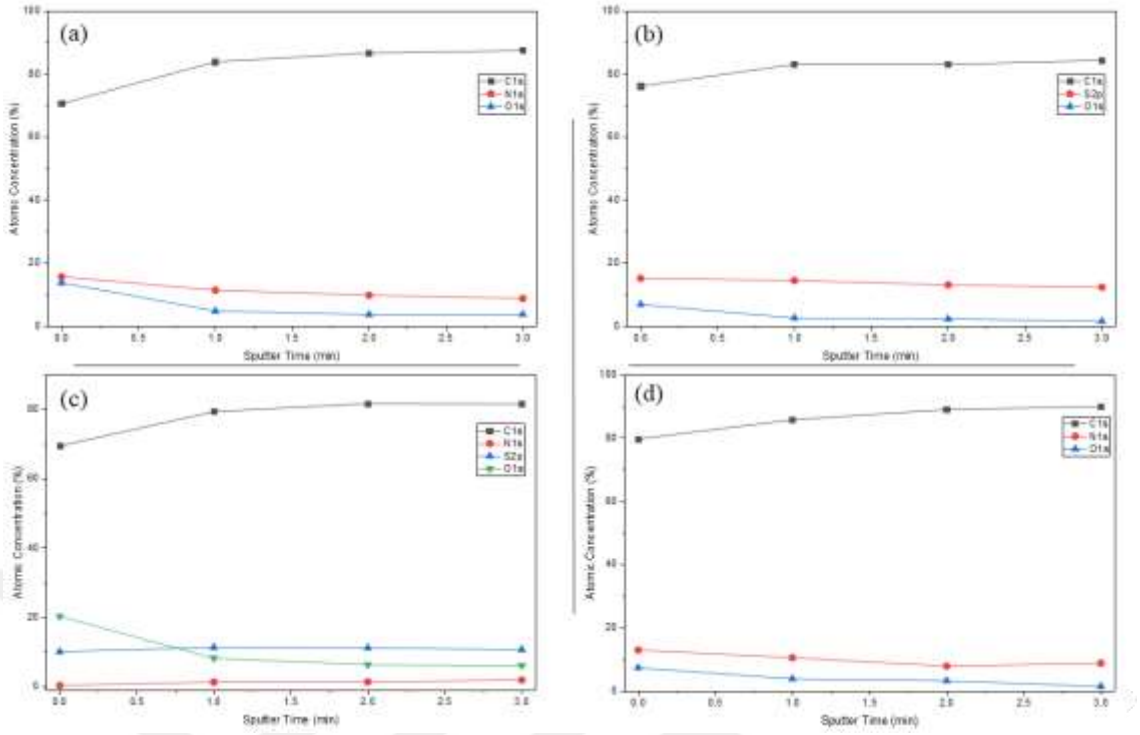

Figure 4.18 XPS depth profiles of (a) polypyrrole, (b) polythiophene, (c) TPP-co-thiophene, and (d) TPP-co-pyrrole thin films

However, when the pyrrole and TPP-co-pyrrole (Figure 4.18 (a) and (d), respectively) thin films are examined, the nitrogen ratio, which was expected to increase with the addition of TPP to the structure, did not increase; this indicates that the polymerization with a 1:1 volume ratio planned in the TPP-co-pyrrole experimental design did not occur and that the pyrrole concentration is much higher. This situation also provides an explanation for why the Q bands expected from TPP were not observed in the UV-Vis spectrum.

4.6 Morphological Characterization of Thin Films Using AFM and SEM

As seen in Figures 4.19 (a) and (b), pyrrole and thiophene thin films are rougher compared to their copolymers. The average roughness (Ra) values are 57.4 nm for the pyrrole thin film and 29.4 nm for the thiophene thin film.

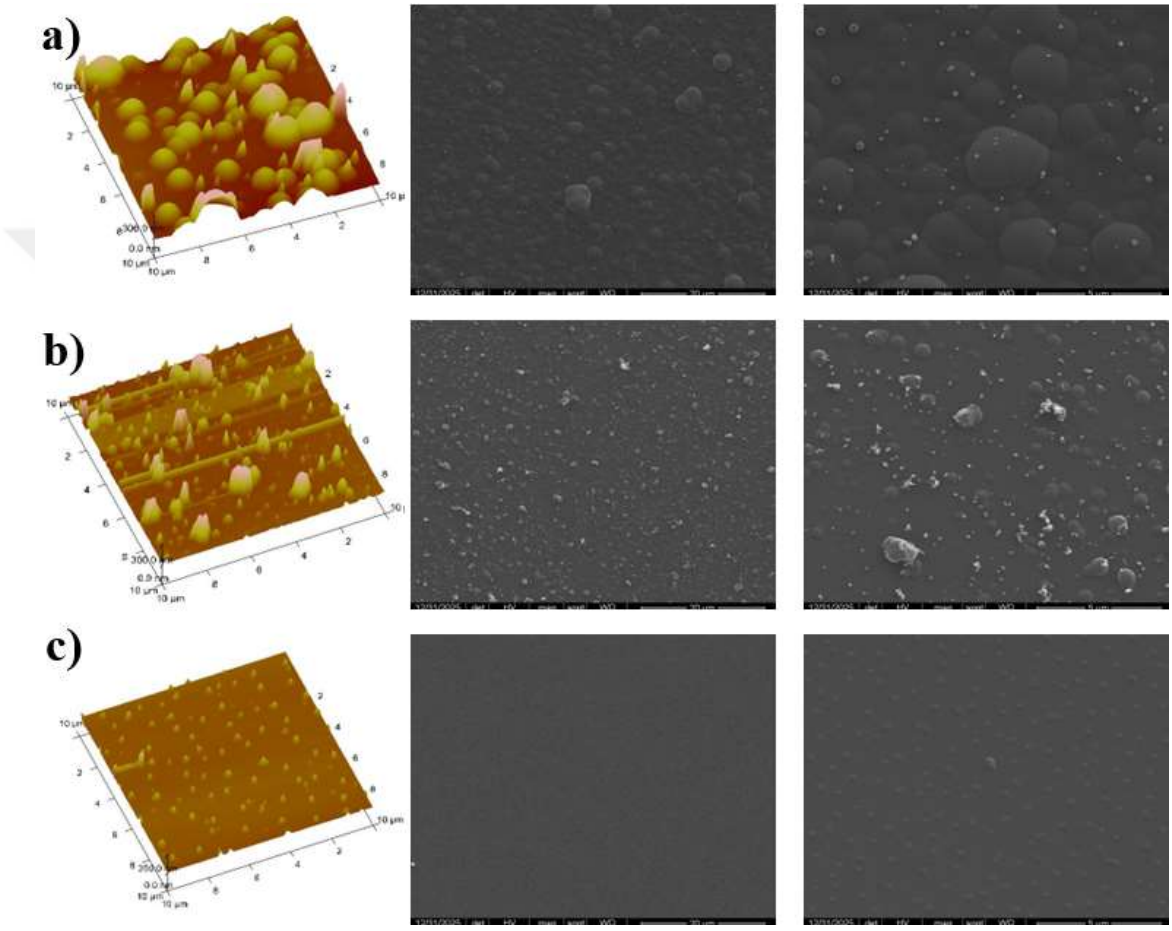

Figure 4.19 AFM and SEM surface morphology images of (a) pyrrole, (b) thiophene, and (c) TPP thin films deposited by PECVD. For each row, the images from left to right correspond to AFM, SEM at 5000× magnification, and SEM at 20000× magnification

After copolymerization with TPP and with each other, the Ra values decrease significantly to 3.47 nm, 0.52 nm, and 0.87 nm for TPP-co-pyrrole, TPP-co-thiophene, and pyrrole-co-thiophene, respectively [as shown in Figures 4.20 (a), (b), and (c), respectively]. Among the homopolymers, the smoothest thin film with the most uniform coverage is the TPP thin film, as shown in Figure 4.19(c), with an Ra value of 4.61 nm.

According to the SEM images, the copolymer films exhibit higher density compared to the homopolymers, and the globular structure typically induced by gas-phase plasma polymerization is less pronounced. The increase in film density is assumed to be caused by an increase in cross-linking bonds within the deposited film (Nagai et al., 1998).

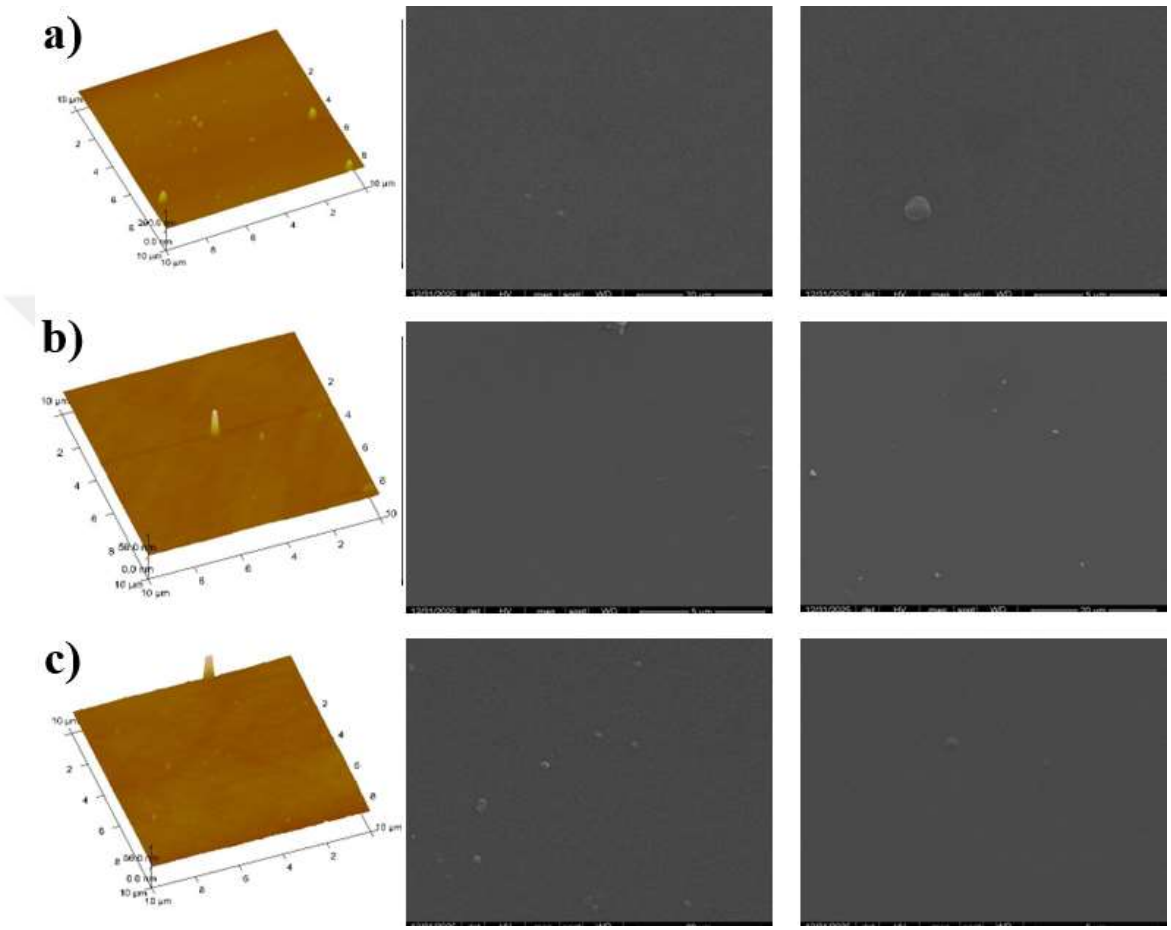

Figure 4.20 AFM and SEM surface morphology images of (a) TPP-co-pyrrole, (b) TPP-co-thiophene, and (c) Pyrrole-co-thiophene thin films deposited by PECVD. For each row, the images from left to right correspond to AFM, SEM at 5000× magnification, and SEM at 20000× magnification

5. CONCLUSION

Within the scope of this thesis, TPP-co-thiophene and TPP-co-pyrrole thin films were successfully produced in order to overcome the wavelength-dependent limitations of conventional photosensitizers in PDT applications. During the fabrication process, plasma-assisted chemical vapor deposition (PECVD) was employed to enable synthesis without the use of any chemicals or solvents other than the active materials. Based on the characterization studies performed on the synthesized films, it was demonstrated as an initial experimental stage that the TPP-co-thiophene thin film could be a promising photosensitizer. On the other hand, studies carried out with pyrrole revealed that the high reactivity and volatility of pyrrole led to significantly higher deposition compared to other monomers during PECVD synthesis. This resulted in the suppression of the characteristic optical properties of TPP and prevented the film from exhibiting absorption at the desired wavelengths. Therefore, further optimization of the PECVD system is required for TPP-co-pyrrole films. Although a similar situation was observed for pyrrole in FTIR studies, it was still evident that pyrrole, like thiophene and TPP, preserved its aromatic structure. FTIR analyses also indicated that the films possessed a cross-linked network structure, as expected from PECVD, suggesting enhanced stability and resistance to aggregation in biological environments.

As a result of the Ultraviolet–Visible (UV–Vis) spectroscopy analysis, it was determined that the TPP–thiophene copolymer thin films exhibit absorption at a wavelength of 655 nm with an approximately 10 nm bathochromic shift in the Soret and Q bands. This critical finding indicates an increase in the conjugation length within the structure and demonstrates that light absorption in the visible region is enhanced in accordance with the objective of deep tissue penetration and will be less affected by the optical masking of melanin pigment. In addition, the broadening of the absorption bands suggests the formation of J-aggregated oligomeric structures, which are advantageous in terms of light-harvesting efficiency. In contrast, for TPP-co-pyrrole films, it was observed that due to the high reactivity and volatility of pyrrole, the optical properties of the polypyrrole matrix were dominant compared to those of TPP and thiophene. Considering the obtained UV–Vis, FTIR, SEM, XPS, and AFM data, it has been demonstrated that the PECVD

method is an effective technique for producing solvent-free photosensitizer films with homogeneous morphology and tunable optical properties suitable for photodynamic therapy applications. It is understood from the SEM and AFM images that the roughness of the homopolymers is higher, while that of the copolymers is lower. Whether the changing surface area due to roughness is an advantage or a disadvantage should be investigated in future studies.

One of the most significant limitations of this study is the need to investigate synthesis parameters that would allow pyrrole/thiophene and TPP to polymerize together at comparable rates. For TPP-co-thiophene films, although a 10 nm red shift can be considered successful for plasma polymerization, it is anticipated that this shift could be further improved through advanced optimization.

Although this thesis successfully presents the synthesis protocols and physicochemical characterizations of the red shifted photosensitizers, its scope remains limited to materials engineering and optical optimization. Therefore, the biological activities of the developed copolymer films are of critical importance for future studies. In addition, although a 10 nm absorption shift was achieved for TPP-co-thiophene, quantitative measurements of singlet oxygen ($^1O_2$) generation are required to verify the photochemical mechanism. Furthermore, cytotoxicity and dark cytotoxicity tests on healthy cells, as well as phototoxicity analyses on melanoma cancer cell lines, should be performed to determine the therapeutic efficacy and biocompatibility of the films. This thesis presents an original, solvent-free, and green fabrication route for stable and optically tunable photosensitizers, paving the way for future studies.

REFERENCES

Abali, H., Celik, I., Karaca, B., Turna, H., Akman, T., Oztop, I., ... ve Kavgaci, H. (2015). Cutaneous melanoma in Turkey: analysis of 1157 patients in the Melanoma Turkish Study. Journal of BU ON.: Official Journal of the Balkan Union of Oncology, 20(4), 1137-1141.

Abu-Thabit, N. Y., ve Makhlouf, A. S. H. (2020). Fundamental of smart coatings and thin films: Synthesis, deposition methods, and industrial applications. In Advances in smart coatings and thin films for future industrial and biomedical engineering applications (pp. 3-35). Elsevier.

Agostinis, P., Berg, K., Cengel, K. A., Foster, T. H., Girotti, A. W., Gollnick, S. O., ... ve Golab, J. (2011). Photodynamic therapy of cancer: an update. CA: a cancer journal for clinicians, 61(4), 250-281.

Alam, M. J., Kapnisis, K., Gilmour, A. D., & Gruber, S. (2023). Toxic or not toxic? The specifications of the standard ISO 10993-5 are not explicit enough to yield comparable results in the cytotoxicity assessment of an identical medical device. Frontiers in Medical Technology, 5, 1195529.

Al-Hamdan, A., Al-Falah, A., & Al-Deri, F. (2022). Comparative Poly2-Formyl (Pyrrole, Furan, & Thiophene): Synthesis, Characterization and Particle Size. Наносистеми, Наноматеріали, Нанотехнології Nanosistemi, Nanomateriali, Nanotehnologii, 20(3), 791–798.

Aratani, N., Osuka, A., Cho, H. S., & Kim, D. (2002). Photochemistry of covalently-linked multi-porphyrinic systems. Journal of Photochemistry and Photobiology C: Photochemistry Reviews, 3(1), 25–52.

Austin, E., ve Jagdeo, J. (2018). An in vitro approach to photodynamic therapy. JoVE (Journal of Visualized Experiments), (138), e58190.

Baba, K., Bengasi, G., El Assad, D., Grysan, P., Lentzen, E., Heinze, K., ... ve Boscher, N. D. (2019). Conductive Directly Fused Poly (Porphyrin) Coatings by Oxidative Chemical Vapour Deposition–From Single-to Triple-Fused. European Journal of Organic Chemistry, 2019(13), 2368-2375.

Baskaran, R., Lee, J., ve Yang, S. G. (2018). Clinical development of photodynamic agents and therapeutic applications. Biomaterials research, 22(1), 25.

Bayram, Ö. (2019). Determination of the Optical Properties of ppTh Nanostructured Films Obtained by RF Plasma Polymerisation Technique. Journal of the Institute of Science and Technology, 9(1), 374–381. https://doi.org/10.21597/JIST.461102

Bengasi, G., Baba, K., Frache, G., Desport, J., Gratia, P., Heinze, K., ve Boscher, N. D. (2019). Conductive fused porphyrin tapes on sensitive substrates by a chemical vapor deposition approach. Angewandte Chemie, 131(7), 2125-2130.

Bhardwaj, V., Gumber, D., Abbot, V., Dhiman, S., & Sharma, P. (2015). Pyrrole: a resourceful small molecule in key medicinal hetero-aromatics. RSC Advances, 5(20), 15233–15266. https://doi.org/10.1039/C4RA15710A

Bouit, P. A., Kamada, K., Feneyrou, P., Berginc, G., Toupet, L., Maury, O., ve Andraud, C. (2009). Two-photon absorption-related properties of functionalized BODIPY dyes in the infrared range up to telecommunication wavelengths. Advanced Materials, 21(10-11), 1151-1154.

Brito, C., Resende, C., ve Oliveira, P. (2016). A 10-Year retrospective analysis of methyl aminolevulinate photodynamic therapy consultation at the hospital de braga. Dermatology and Therapy, 6, 265-272.

Broekgaarden, M., Zhang, H., Korbelik, M., Hamblin, M. R., ve Heger, M. (Eds.). (2022). Photodynamic Therapy: Methods and Protocols. Humana Press.

Bronaugh, R. L., ve Maibach, H. I. (Eds.). (1999). Percutaneous absorption: drugs--cosmetics--mechanisms--methodology: drugs--cosmetics--mechanisms--methodology. CRC Press

Cai, H., Wang, Y. X., Zheng, J. C., Sun, P., Yang, Z. Y., Li, Y. L., ... ve Liu, W. (2015). Photodynamic therapy in combination with CO 2 laser for the treatment of Bowen's disease. Lasers in medical science, 30, 1505-1510.

Calixto, G. M. F., Bernegossi, J., De Freitas, L. M., Fontana, C. R., Chorilli, M., & Grumezescu, A. M. (2016). Nanotechnology-based drug delivery systems for photodynamic therapy of cancer: A review. Molecules, 21(3). https://doi.org/10.3390/MOLECULES21030342

Castano, A. P., Demidova, T. N., ve Hamblin, M. R. (2004). Mechanisms in photodynamic therapy: part one—photosensitizers, photochemistry and cellular localization. Photodiagnosis and Photodynamic Therapy, 1(4), 279-293.

Ceylan, C., Oztürk, G., ve Alper, S. (2003). Non-Melanoma Skin Cancers between the Years of 1990 and 1999 in Izmir, Turkey: Demographic and Clinicopathological Characteristics. The Journal of Dermatology, 30(2), 123-131.

Champeau, M., Vignoud, S., Mortier, L., ve Mordon, S. (2019). Photodynamic therapy for skin cancer: How to enhance drug penetration? Journal of photochemistry and photobiology. B, Biology, 197.

Cho, S. J., & Boo, J. H. (2012). A study on the characteristics of plasma polymer thin film with controlled nitrogen flow rate. Nanoscale Research Letters 2012 7:1, 7(1), 62-. https://doi.org/10.1186/1556-276X-7-62

Ciążyńska, M., Kamińska-Winciorek, G., Lange, D., Lewandowski, B., Reich, A., Sławińska, M., Pabianek, M., Szczepaniak, K., Hankiewicz, A., Ułańska, M., Morawiec, J., Błasińska-Morawiec, M., Morawiec, Z., Piekarski, J., Nejc, D., Brodowski, R., Zaryczańska, A., Sobjanek, M., Nowicki, R. J., … Lesiak, A.

(2021). The incidence and clinical analysis of non-melanoma skin cancer. Scientific Reports 2021 11:1, 11(1), 1-10.

Cruz, G. J., Morales, J., & Olayo, R. (1999). Films obtained by plasma polymerization of pyrrole. Thin Solid Films, 342(1–2), 119–126. https://doi.org/10.1016/S0040-6090(98)01450-3

Çoşğun, A., Taşçioğlu, A., Yilmaz, G., Mehmet Akif Ersoy Üniversitesi, B., ve Bilimleri Enstitüsü, F. (2021). İnce Film Üretiminde Kimyasal Buhar Biriktirme Yöntemi ve Çeşitleri. The Journal of Graduate School of Natural and Applied Sciences of Mehmet Akif Ersoy University, 12(2), 351-363.

Dams, R., Vangeneugden, D., & Vanderzande, D. (2006). Plasma deposition of thiophene derivatives under atmospheric pressure. Wiley Online LibraryR Dams, D Vangeneugden, D VanderzandeChemical Vapor Deposition, 2006•Wiley Online Library, 12(12), 719–727. https://doi.org/10.1002/CVDE.200606483

Dianatdar, A., ve Bose, R. K. (2023). Oxidative chemical vapor deposition for synthesis and processing of conjugated polymers: a critical review. Journal of Materials Chemistry C, 11(35), 11776-11802.

Dinache, A., Nistorescu, S., Tozar, T., Smarandache, A., Boni, M., Prepelita, P., Staicu, A., Dinache, A., Nistorescu, S., Tozar, T., Smarandache, A., Boni, M., Prepelita, P., & Staicu, A. (2022). Spectroscopic Investigations of Porphyrin-TiO2 Nanoparticles Complexes. Molecules 2023, Vol. 28, 28(1). https://doi.org/10.3390/MOLECULES28010318

Ding, H., Yu, H., Dong, Y., Tian, R., Huang, G., Boothman, D. A., Sumer, B. D., ve Gao, J. (2011). Photoactivation switch from type II to type I reactions by electron-rich micelles for improved photodynamic therapy of cancer cells under hypoxia. Journal of Controlled Release, 156(3), 276-280.

Dougherty, T. J., Gomer, C. J., Henderson, B. W., Jori, G., Kessel, D., Korbelik, M., ... ve Peng, Q. (1998). Photodynamic therapy. Journal of National Cancer Institute, 90(12), 889-905.

DURSUN, E., KORKMAZ, H., BAYIZ, Ü., SAMİM, E., ve ÖZERİ, C. (2002). Baş ve boyun bölgesinin melanoma dışı cilt kanserleri. KBB ve BBC Dergisi, 10(3), 156-163.

Elçin, G. (2015). Deri Tümörlerinin Cerrahi Tedavisi. Turkish Journal of Dermatology/Turk Dermatoloji Dergisi, 9(2).

Elçin, G. (2015). Mohs mikrografik cerrahisi: Türkiye'de olsa ne olur, olmasa ne olur?/Mohs micrographic surgery: What if there is no Mohs micrographic surgery in Turkey?. Türkderm: Türk Deri Hastalıkları ve Frengi Arşivi= Turkderm: Turkish Archives of Dermatology and Venereology, 49(4), 236.

El-Nahass, M., Zeyada, H., Aziz, M., & Makhlouf, M. (2005). Effect of High Energy X-ray Irradiation on the Optical Properties of Tetraphenylporphyrin.

Ersoy, ACER ve Erdoğan, H. K. (2019). SIK GÖRÜLEN DERİ KANSERLERİNİN EPİDEMİYOLOJİSİ. ESTÜDAM Halk Sağlığı Dergisi, 4, 52-60.

Fırnhaber, J. M. (2012). Diagnosis and Treatment of Basal Cell and Squamous Cell Carcinoma. American Family Physician, 86(2), 161-168.

Fritsch, C., Goerz, G., ve Ruzicka, T. (1998). Photodynamic therapy in dermatology. Archives of dermatology, 134(2), 207-214.

Gamsizkan, M., Yilmaz, I., Buyukbabani, N., Demirkesen, C., Demiriz, M., Cetin, E. D., Ince, U., Akalin, T., Demirkan, N. C., Lebe, B., Erdem, O., Gokoz, O., Sakiz, D., Demireli, P. T., Astarci, H. M., Adim, S. B., Zemheri, I. E., Acikalin, A., Yaman, B., … Bassorgun, C. I. (2014). A retrospective multicenter evaluation of cutaneous melanomas in Turkey. Asian Pacific journal of cancer prevention : APJCP, 15(23), 10451-10456.

Gareau, D. S., Krueger, J. G., Hawkes, J. E., Lish, S. R., Dietz, M. P., Mülberger, A. G., ... ve Carucci, J. A. (2017). Line scanning, stage scanning confocal microscope (LSSSCM). Biomedical Optics Express, 8(8), 3807-3815.

Gelfuso, G. M., Gratieri, T., Souza, J. G., Thomazine, J. A., ve Lopez, R. F. V. (2011). The influence of positive or negative charges in the passive and iontophoretic skin penetration of porphyrins used in photodynamic therapy. European Journal of Pharmaceutics and Biopharmaceutics, 77(2), 249-256.

Gharahcheshmeh, M. H., Tavakoli, M. M., Gleason, E. F., Robinson, M. T., Kong, J., ve Gleason, K. K. (2019). Tuning, optimization, and perovskite solar cell device integration of ultrathin poly(3,4-ethylene dioxythiophene) films via a single-step all-dry process. Science Advances, 5(11).

Gibbons, D. J., Boh, A., Habermeyer, B., Villandier, N., Leroy-Lhez, S., ve Williams, R. M. (2022). Photo-activated thin films of porphyrins for reactive oxygen species generation. Journal of Porphyrins and Phthalocyanines, 26(8), 550-562.

Goktas, H., Ince, F. G., Iscan, A., Yildiz, I., Kurt, M., & Kaya, I. (2009). The molecular structure of plasma polymerized thiophene and pyrrole thin films produced by double discharge technique. Synthetic Metals, 159(19–20), 2001–2008.

Gratieri, T., Alberti, I., Lapteva, M., ve Kalia, Y. N. (2013). Next generation intra- and transdermal therapeutic systems: Using non- and minimally-invasive technologies to increase drug delivery into and across the skin. European Journal of Pharmaceutical Sciences, 50(5), 609-622.

Groenewoud, L. M. H., Engbers, G. H. M., Terlingen, J. G. A., Wormeester, H., & Feijen, J. (2000). Pulsed Plasma Polymerization of Thiophene. Langmuir, 16(15), 6278–6286.

Gupta, S., Dwarakanath, B. S., Muralidhar, K., ve Jain, V. (2003). Cellular uptake, localization and photodynamic effects of haematoporphyrin derivative in human

glioma and squamous carcinoma cell lines. Journal of Photochemistry and Photobiology B: Biology, 69(2), 107-120.

Hakverdi, S., Balci, D. D., Dogramaci, C. A., Toprak, S., ve Yaldiz, M. (2011). Retrospective analysis of basal cell carcinoma. Indian Journal of Dermatology, Venereology and Leprology, 77, 251.

Heier, P., Boscher, N. D., Bohn, T., Heinze, K., ve Choquet, P. (2014). A new class of Zn II and Cr III porphyrins incorporated into porous polymer matrices via an atmospheric pressure plasma enhanced CVD to form gas sensing layers. Journal of Materials Chemistry A, 2(5), 1560-1570.

Herkenne, C., Naik, A., Kalia, Y. N., Hadgraft, J., ve Guy, R. H. (2006). Pig ear skin ex vivo as a model for in vivo dermatopharmacokinetic studies in man. Pharmaceutical Research, 23(8), 1850-1856.

Inagaki, N. (2006). Polymer Films Produced by Plasma Polymerization. Materials Surface Processing by Directed Energy Techniques, 659–707.

Iriyama, Y., & Wa, M. H. (2001). Plasma Polymerization of Pyrrole and Structures and Properties of the Polymerized Films. Polymer Journal, 33(5), 419–423.

Jain, N. K., Sawant, M. S., Nikam, S. H., ve Jhavar, S. (2016). Metal deposition: Plasma-based processes. Encyclopedia of Plasma Technology, 1st ed.; Taylor and Francis: New York, NY, USA, 722-740.

Jeelan Basha, N., Basavarajaiah, S. M., & Shyamsunder, K. (2022). Therapeutic potential of pyrrole and pyrrolidine analogs: an update. Molecular Diversity 2022 26:5, 26(5), 2915-2937.

Jeremic, G., Brandt, M. G., Jordan, K., Doyle, P. C., Yu, E., ve Moore, C. C. (2011). Using photodynamic therapy as a neoadjuvant treatment in the surgical excision of nonmelanotic skin cancers: prospective study. Journal of Otolaryngology-Head ve Neck Surgery= Le Journal D'oto-rhino-laryngologie et de Chirurgie Cervico-faciale, 40, S82-9.

Juvekar, V., Cao, Y., Koh, C. W., Lee, D. J., Kwak, S. Y., Kim, S. M., ... & Kim, H. M. (2024). Overcoming melanin interference in melanocyte photodynamic therapy with a pyrene-derived two-photon photosensitizer. Chemical Engineering Journal, 493, 152796.

Kalal, B. S., Upadhya, D., ve Pai, V. R. (2017). Chemotherapy Resistance Mechanisms in Advanced Skin Cancer. Oncology Reviews, 11(1), 19-25.

Kamal, M. M., & Bhuiyan, A. H. (2013). Thickness dependent direct current electrical conduction in plasma polymerized pyrrole monolayer thin films. Advanced Materials Research, 741, 59–64.

Karagas, M. R., Stukel, T. A., Greenberg, E. R., Baron, J. A., Mott, L. A., ve Stern, R. S. (1992). Risk of Subsequent Basal Cell Carcinoma and Squamous Cell Carcinoma of the Skin Among Patients With Prior Skin Cancer. JAMA, 267(24), 3305-3310.

Kasap, Ş., Pektaş, M. L., Yelda, D. E. R. E., ve ALTIPARMAK, M. (2015). Muğla'daki Cilt Kanseri Olgularının Retrospektif Değerlendirilmesi. Muğla Sıtkı Koçman Üniversitesi Tıp Dergisi, 2(3), 34-37.

Khong, J., Gorayski, P., ve Roos, D. (2020). Non-melanoma skin cancer in general practice: Radiotherapy is an effective treatment option. Australian Journal of General Practice, 49(8), 496-499.

Kim, B. F., & Bohandy, J. (1981). SPECTROSCOPY OF PORPHYRINS. Johns Hopkins A PL Technical Digest, 2(3), 153–163.

Kong, C., ve Chen, X. (2022). Combined Photodynamic and Photothermal Therapy and Immunotherapy for Cancer Treatment: A Review. International Journal of Nanomedicine, 17, 6427-6446.

Kravets, L., Dmitriev, S., Lizunov, N., Satulu, V., Mitu, B., & Dinescu, G. (2010). Properties of poly(ethylene terephthalate) track membranes with a polymer layer obtained by plasma polymerization of pyrrole vapors. Nuclear Instruments and Methods in Physics Research Section B: Beam Interactions with Materials and Atoms, 268(5), 485–492.

Kulkarni, S. (2018). Plasma Assisted Polymer Synthesis and Processing. Non-Thermal Plasma Technology for Polymeric Materials: Applications in Composites, Nanostructured Materials, and Biomedical Fields, 67–93. https://doi.org/10.1016/B978-0-12-813152-7.00003-2

Kurochkin, I. Y., Olshevskaya, V. A., Zaitsev, A. V., Giricheva, N. I., ve Girichev, G. V. (2021). Vibrational Spectrum of 5,10,15,20-Tetraphenylporphyrin (H2 TPP) and Platinum(II) 5,10,15,20-Tetra(phenyl/pentafluorophenyl) porphyrins (PtTPP and PtTF5 PP). Macroheterocycles, 14(4), 334-341.

Lam, M. W., Wells, H., Gibbs, H., Zhao, A., Tso, S., & Wernham, A. (2024). P051 The what, how and why of basal cell carcinoma: natural progression and surgical intervention. British Journal of Dermatology, 191(Supplement_1), i38-i38.

Lee, C. N., Hsu, R., Chen, H., ve Wong, T. W. (2020). Daylight Photodynamic Therapy: An Update. Molecules, 25(21).

Lee, E. H., Klassen, A. F., Lawson, J. L., Cano, S. J., Scott, A. M., ve Pusic, A. L. (2016). Patient experiences and outcomes following facial skin cancer surgery: A qualitative study. Australasian Journal of Dermatology, 57(3), e100-e104.

Liu, R., & Liu, Z. (2009). Polythiophene: Synthesis in aqueous medium and controllable morphology. Chinese Science Bulletin, 54(12), 2028-2032.

Lu, Y. gang, Wang, Y. yuan, Yang, Y. dong, Zhang, X. cun, Gao, Y., Yang, Y., Zhang, J. bo, ve Li, G. ling. (2014). Efficacy of topical ALA-PDT combined with excision in the treatment of skin malignant tumor. Photodiagnosis and Photodynamic Therapy, 11(2), 122-126.

Lucena, S. R., Salazar, N., Gracia-Cazaña, T., Zamarrón, A., González, S., Juarranz, Á., ve Gilaberte, Y. (2015). Combined treatments with photodynamic therapy for non-melanoma skin cancer. International Journal of Molecular Sciences, 16(10), 25912-25933.

Makhlouf, M. M., El-Denglawey, A., Zeyada, H. M., & El-Nahass, M. M. (2014). The structural and optical characterizations of tetraphenylporphyrin thin films. Journal of Luminescence, 147, 202–208. https://doi.org/10.1016/J.JLUMIN.2013.11.007

Mishra, R., Jha, K. K., Kumar, S., & Tomer, I. (2011). Scholars Research Library Synthesis, properties and biological activity of thiophene: A review. Der Pharma Chemica, 3(4), 38–54.

Morton, C. A., Szeimies, R. M., Basset-Seguin, N., Calzavara-Pinton, P., Gilaberte, Y., Hædersdal, M., Hofbauer, G. F. L., Hunger, R. E., Karrer, S., Piaserico, S., Ulrich, C., Wennberg, A. M., ve Braathen, L. R. (2019). European Dermatology Forum guidelines on topical photodynamic therapy 2019 Part 1: treatment delivery and established indications – actinic keratoses, Bowen's disease and basal cell carcinomas. Journal of the European Academy of Dermatology and Venereology, 33(12), 2225-2238.

Mustari, A., Nishidate, I., Wares, M. A., Maeda, T., Kawauchi, S., Sato, S., Sato, M., ve Aizu, Y. (2018). Agarose-based Tissue Mimicking Optical Phantoms for Diffuse Reflectance Spectroscopy. JoVE (Journal of Visualized Experiments), 2018(138), e57578.

Nageswaran, G., Jothi, L., & Jagannathan, S. (2018). Plasma Assisted Polymer Modifications. Non-Thermal Plasma Technology for Polymeric Materials: Applications in Composites, Nanostructured Materials, and Biomedical Fields, 95–127. https://doi.org/10.1016/B978-0-12-813152-7.00004-4

Nakano, A., Watanabe, D., Akita, Y., Kawamura, T., Tamada, Y., ve Matsumoto, Y. (2011). Treatment efficiency of combining photodynamic therapy and ionizing radiation for Bowen's disease. Journal of the European Academy of Dermatology and Venereology, 25(4), 475-478.

National Cancer Institute. (2021). Skin Cancer Treatment (PDQ®). Board, PDQ Adult Treatment Editorial, 2(7), 1-9.

Neville, J. A., Welch, E., ve Leffell, D. J. (2007). Management of nonmelanoma skin cancer in 2007. Nature Clinical Practice Oncology 2007 4:8, 4(8), 462-469.

Ng, S. F., Rouse, J. J., Sanderson, F. D., Meidan, V., ve Eccleston, G. M. (2010). Validation of a static Franz diffusion cell system for in vitro permeation studies. AAPS PharmSciTech, 11(3), 1432-1441.

Odobel, F., Suresh, S., Blart, E., Nicolas, Y., Quintard, J. P., Janvier, P., ... & Hammarström, L. (2002). Synthesis of oligothiophene-bridged bisporphyrins and study of the linkage dependence of the electronic coupling. Chemistry–A European Journal, 8(13), 3027-3046.

Oseroff, A. R., Blumenson, L. R., Wilson, B. D., Mang, T. S., Bellnier, D. A., Parsons, J. C., Frawley, N., Cooper, M., Zeitouni, N., & Dougherty, T. J. (2006). A dose ranging study of photodynamic therapy with porfimer sodium (Photofrin®) for treatment of basal cell carcinoma. Lasers in Surgery and Medicine, 38(5), 417-426.

Park, C. K., Kim, Y. H., Hwangbo, S., ve Cho, H. (2017). Photodynamic therapy by conjugation of cell-penetrating peptide with fluorochrome. International Journal of Nanomedicine, 12, 8185-8196.

Pathak, P., Zarandi, M. A., Zhou, X., & Jayawickramarajah, J. (2021). Synthesis and Applications of Porphyrin-Biomacromolecule Conjugates. Frontiers in Chemistry, 9, 764137.

Philkhana, S. C., Badmus, F. O., Dos Reis, I. C., & Kartika, R. (2021). Recent Advancements in Pyrrole Synthesis. Synthesis, 53(09), 1531–1555. https://doi.org/10.1055/S-0040-1706713

Pyne, J. H., Myint, E., Barr, E. M., Clark, S. P., & Hou, R. (2018). Basal cell carcinoma: variation in invasion depth by subtype, sex, and anatomic site in 4,565 cases. Dermatology Practical & Conceptual, 8(4), 314.

Quiroz-Segoviano, R. I. Y., García-Sánchez, M. A., Delgado-Buenrostro, N. L., Chirino, Y. I., Bernal-Chávez, S., Nava-Arzaluz, M. G., & Ganem-Rondero, A. (2019). Tetraphenylporphyrin intended for use in photodynamic therapy: Influence of sonophoresis and the formulation (solution or microemulsion) on percutaneous penetration. Journal of Drug Delivery Science and Technology, 53.

Ravve, A. (2013). Principles of polymer chemistry. Springer Science and Business Media.

Ross, A., Pasula, R., ve Hornak, L. (2009). Exploring multispectral iris recognition beyond 900nm. IEEE 3rd International Conference on Biometrics: Theory, Applications and Systems, BTAS 2009.

Sakthi Kumar, D., Nakamura, K., Nishiyama, S., Ishii, S., Noguchi, H., Kashiwagi, K., & Yoshida, Y. (2003). Optical and electrical characterization of plasma polymerized pyrrole films. Journal of Applied Physics, 93(5), 2705–2711. https://doi.org/10.1063/1.1542692

Satyanarayana Reddy Karri, V., Vinothkumar, G., Sivarajakumar, R., ve Venkata Satyanarayana Reddy Karri, V. (2017). Skin Cancer: Current Treatments, Limitations and the Role of Polymeric Nano Particles for the Effective Treatment of Skin Cancer. JSM Nanotechnol Nanomed, 5(3), 1055.

Schmults, C. D., Karia, P. S., Carter, J. B., Han, J., ve Qureshi, A. A. (2013). Factors predictive of recurrence and death from cutaneous squamous cell carcinoma: a 10-year, single-institution cohort study. JAMA dermatology, 149(5), 541-547.

Shabbir, H., Dellago, C., ve Hartmann, M. A. (2019). A high coordination of cross-links is beneficial for the strength of cross-linked fibers. Biomimetics, 4(1), 12.

Sharma, S. K., Huang, Y.-Y., Hamblin, M. R., Hamblin, M. R., Sharma, S. K., Huang, Y.-Y., ve Hamblin, · M R. (2015). Melanoma Resistance to Photodynamic Therapy. 229-246.

Sholl, D. S., ve Steckel, J. A. (2022). Density functional theory: a practical introduction. John Wiley ve Sons.

Simões, M. C. F., Sousa, J. J. S., ve Pais, A. A. C. C. (2015). Skin cancer and new treatment perspectives: A review. Cancer Letters, 357(1), 8-42.

Sotiriou, E., Apalla, Z., Vrani, F., Lallas, A., Chovarda, E., ve Ioannides, D. (2015). Photodynamic therapy vs. imiquimod 5% cream as skin cancer preventive strategies in patients with field changes: A randomized intraindividual comparison study. Journal of the European Academy of Dermatology and Venereology, 29(2), 325-329.

Sotiriou, E., Lallas, A., Apalla, Z., ve Ioannides, D. (2011). Treatment of giant Bowen's disease with sequential use of photodynamic therapy and imiquimod cream. Photodermatology, Photoimmunology ve Photomedicine, 27(3), 164-166.

Sousa, S. F., Fernandes, P. A., ve Ramos, M. J. (2007). General performance of density functionals. The Journal of Physical Chemistry A, 111(42), 10439-10452.

Souto, E. B., da Ana, R., Vieira, V., Fangueiro, J. F., Dias-Ferreira, J., Cano, A., Zielińska, A., Silva, A. M., Staszewski, R., ve Karczewski, J. (2022). Non-melanoma skin cancers: physio-pathology and role of lipid delivery systems in new chemotherapeutic treatments. Neoplasia, 30, 100810.

Sümen, A ve Öncel, S. (2018). Türkiye'de Cilt Kanseri ve Güneşten Korunmaya Yönelik Yapılan Araştırmaların İncelenmesi. Turkiye Klinikleri Journal of Nursing Sciences, 10(1).

Şen, P., Hirel, C., Andraud, C., Aronica, C., Bretonnière, Y., Mohammed, A., Ågren, H., Minaev, B., Minaeva, V., Baryshnikov, G., Lee, H.-H., Duboisset, J., Lindgren, M., Şen, P., Hirel, C., Andraud, C., Aronica, C., Bretonnière, Y., Mohammed, A., … Lindgren, M. (2010). Fluorescence and FTIR Spectrum Analysis of Trans-A2B2-Substituted Di- and Tetra-Phenyl Porphyrins. Materials 2010, Vol. 3, Pages 4446-4475, 3(8), 4446–4475.

Tan, Y., & Ghandi, K. (2013). Kinetics and mechanism of pyrrole chemical polymerization. Synthetic Metals, 175, 183–191.

Taniguchi, M., Lindsey, J. S., Bocian, D. F., & Holten, D. (2021). Comprehensive review of photophysical parameters (ε, Φf, τs) of tetraphenylporphyrin (H2TPP) and zinc tetraphenylporphyrin (ZnTPP) – Critical benchmark molecules in photochemistry and photosynthesis. Journal of Photochemistry and Photobiology C: Photochemistry Reviews, 46, 100401.

Thakur, S., Kumar, D., Jaiswal, S., Goel, K. K., Rawat, P., Srivastava, V., Dhiman, S., Jadhav, H. R., & Dwivedi, A. R. (2024). Medicinal chemistry-based perspectives on thiophene and its derivatives: exploring structural insights to discover plausible druggable leads. RSC Medicinal Chemistry.

Titov, V. A., Krivykh, E. S., Ageeva, T. A., Shikova, T. G., Solov'Eva, A. B., Timofeeva, V. A., Vershinina, I. A., Rybkin, V. V., & Choi, H. S. (2008). Immobilization of tetraphenylporphyn and its metallocomplexes on the surface of plasma-treated polypropylene. SpringerVA Titov, ES Krivykh, TA Ageeva, TG Shikova, AB Solov'eva, VA Timofeeva, IA VershininaPolymer Science Series A, 2008•Springer, 50(8), 841–847.

Touloupas, I., Weyandt, E., Meijer, E. W., & Hildner, R. (2023). Unusual Photophysical Properties of Porphyrin-Based Supramolecular Polymers Unveiled: The Role of Metal Ligands and Side Group Amide Connectivity. The Journal of Physical Chemistry. C, Nanomaterials and Interfaces, 127(48), 23323.

Varol, M. (2020). Photodynamic therapy assay. Methods in Molecular Biology, 2109, 241-250.

Vianna Lopez, R. F., Lange, N., Guy, R., ve Bentley, M. V. L. B. (2004). Photodynamic therapy of skin cancer: controlled drug delivery of 5-ALA and its esters. Advanced Drug Delivery Reviews, 56(1), 77-94.

Villari, V., Mineo, P., Scamporrino, E., & Micali, N. (2012). Role of the hydrogen-bond in porphyrin J-aggregates. RSC Advances, 2(33), 12989–12998.

Wachowska, M., Muchowicz, A., Firczuk, M., Gabrysiak, M., Winiarska, M., Wańczyk, M., Bojarczuk, K., ve Golab, J. (2011). Aminolevulinic acid (ala) as a prodrug in photodynamic therapy of cancer. Molecules, 16(5), 4140-4164.

Wang, J., Neoh, K. G., & Kang, E. T. (2004). Comparative study of chemically synthesized and plasma polymerized pyrrole and thiophene thin films. Thin Solid Films, 446(2), 205–217.

Wang, Z., Che, J., ve Ye, C. (2010). Application of ferric chloride both as oxidant and complexant to enhance the dissolution of metallic copper. Hydrometallurgy, 105(1-2), 69-74.

Yasuda, H. K. (2005). Some important aspects of plasma polymerization. Plasma Processes and Polymers, 2(4), 293–304.

Yuan, W. Z., Lu, P., Chen, S., Lam, J. W., Wang, Z., Liu, Y., ... & Tang, B. Z. (2010). Changing the behavior of chromophores from aggregation-caused quenching to

aggregation-induced emission: development of highly efficient light emitters in the solid state. Advanced materials, 22(19), 2159-2163.

Zeinali, S., Tuncel, A., Yüzer, A., ve Yurt, F. (2021). Imaging and detection of cell apoptosis by In vitro photodynamic therapy applications of zinc (II) phthalocyanine on human melanoma cancer. Photodiagnosis and Photodynamic Therapy, 36, 102518.

Zhang, J., Wu, M. Z., Pu, T. S., Zhang, Z. Y., Jin, R. P., Tong, Z. S., Zhu, D. Z., Cao, D. X., Zhu, F. Y., & Cao, J. Q. (1997). Investigation of the plasma polymer deposited from pyrrole. Thin Solid Films, 307(1–2), 14–20.

Zhang, K., Liu, J., Zhang, Y., Fan, J., Wang, C. K., & Lin, L. (2019). Theoretical study of the mechanism of aggregation-caused quenching in near-infrared thermally activated delayed fluorescence molecules: hydrogen-bond effect. The Journal of Physical Chemistry C, 123(40), 24705-24713.

Zheng, N., Li, X., Huangfu, S., Xia, K., Yue, R., Wu, H., ve Song, W. (2021). Linear and high-molecular-weight poly-porphyrins for efficient photodynamic therapy. Biomaterials Science, 9(13), 4630-4638.

Zhuang, Z., Dai, J., Yu, M., Li, J., Shen, P., Hu, R., Lou, X., Zhao, Z., ve Tang, B. Z. (2020). Type I photosensitizers based on phosphindole oxide for photodynamic therapy: apoptosis and autophagy induced by endoplasmic reticulum stress. Chemical Science, 11(13), 3405-3417.